Integrated Modeling of Carbon and Boron Nitride Nanotubes Synthesis in Plasma of High-Pressure Arc

Igor D. Kaganovich, Jian Chen, Alexander Khrabry, Andrei Khodak, Yuri Barsukov*, Omesh Dwivedi, Sierra Jubin, Mikael Tacu, Stephane Ethier**

Princeton Plasma Physics Laboratory, USA
***Peter the Great St. Petersburg State University, Russia**
****CEA de Bruyeres-le-Chatel, France**

GEC meeting, October 9, 2020

U.S. DEPARTMENT OF ENERGY | Office of Science

PPPL PRINCETON PLASMA PHYSICS LABORATORY

PRINCETON UNIVERSITY

Outline

nano.pppl.gov

- **Motivation: Develop understanding how nanomaterial grow and identify plasma conditions in the synthesis area**
- **Modeling of arc structure**
- **Modeling of nanoparticle nucleation and growth**
- **Atomistic simulations of key processes of nanotube growth**
  - **Carbon nanomaterials**
  - **Boron-Nitride nanomaterials**
- **Summary**

Plasma Science Studies of Nanomaterial Synthesis

- **Goal: Uncover long standing puzzle how carbon and boron nitride nanotubes grow in plasma synthesis.**
- **Devices: Plasma arc and DC or RF plasma torches, laser-ablation.**
- **Approach: Perform detailed characterization of plasma and nanoparticles parameters using laser diagnostics; develop integrated and validated models comprised of numerical tools capable of simulating nucleation of nano-material growth and particle transport and plasma properties.**

Images of boron-nitride nanotubes and boron catalyst particles.

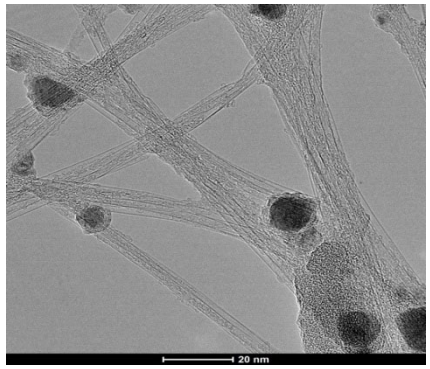

Arc as a versatile method of nanomaterial synthesis

- **Many nanostructures were synthesized at different arc conditions: C60, MWCNT, SWNT, graphene flakes, nanofibers**
- **A graphite anode provides carbon feedstock to produce plasma and nanomaterials.**

See M. Keidar and I. Beilis, Plasma Engineering

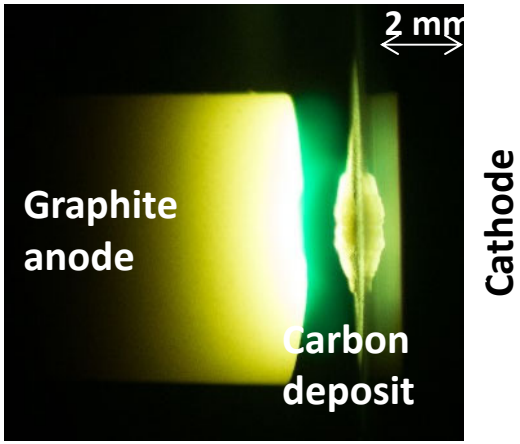

1-2 kW input power, Helium buffer gas, atmospheric pressure.

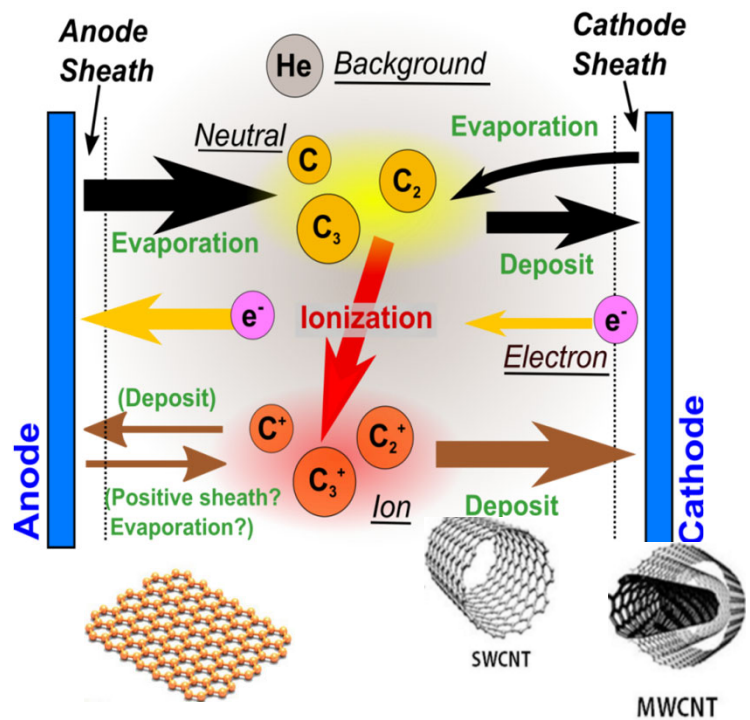

Fundamental Studies of Synthesis of Nanomaterials: A joint challenge for plasma and materials sciences

A central objective of the research is to understand the synergistic roles of plasma and materials processes in arc synthesis of Carbon and Boron Nitride (BN) nanotubes (CNTs, BNNTs)

- **Characterization of the plasma**
- **In-situ laser diagnostics of nanoparticles**
- **Ex-situ diagnostics of nanoparticles**
- **Development, validation, and integration of codes for multi-scale modeling of plasma nanomaterial synthesis.**

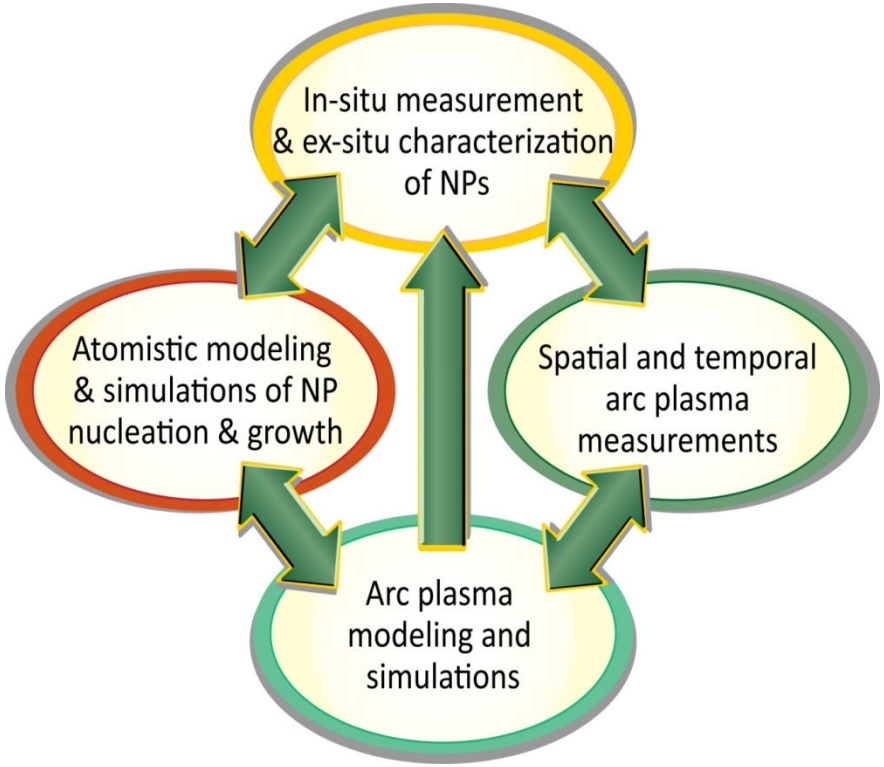

Computational tools used for simulations of arc plasma and nucleation and growth of nanostructures

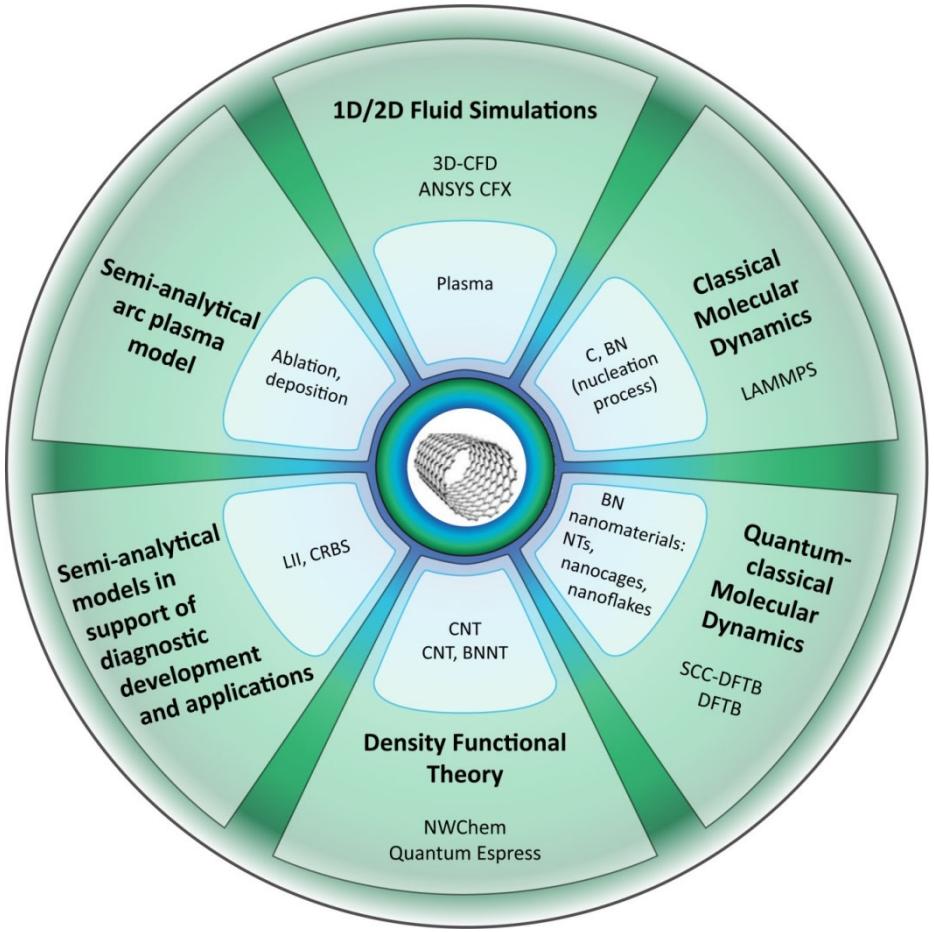

Outline

- **Modeling of arc structure**

What are conditions for carbon arc nanomaterial synthesis?

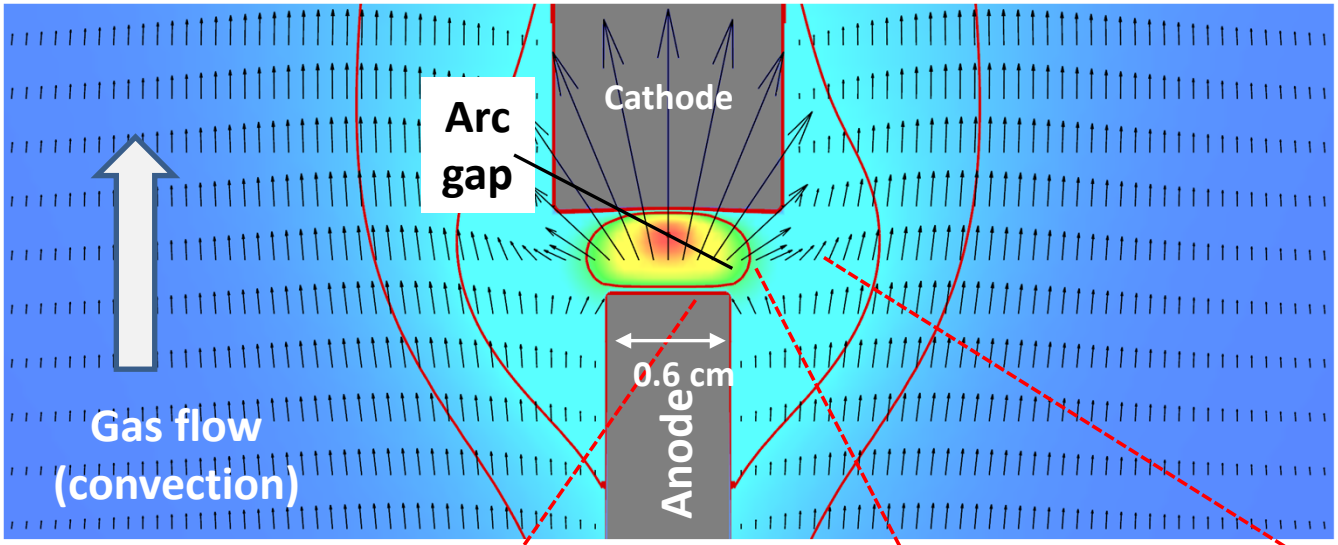

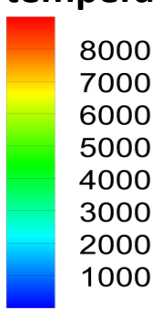

T = 4000 K

Evaporation, Dissociation

$C \approx 10^{17} - 10^{18}$ cm^{-3}

$He \approx 3 \cdot 10^{17}$ cm^{-3}

$C^{+} \approx 10^{14} - 3 \cdot 10^{16}$ cm^{-3}

T = 3000 K

Clusters, nucleation

$C \approx 10^{15} - 10^{16}$ cm^{-3}

$He \approx 3 \cdot 10^{18}$ cm^{-3}

$C^{+} \sim 10^{12}$ cm^{-3}

T = 2000 K

Growth, bundling

$C \approx 10^{14} - 10^{15}$ cm^{-3}

$He > 3 \cdot 10^{18}$ cm^{-3}

$C^{+} \approx 10^{10}$ cm^{-3}

Governing plasma equations

2D-3D model, C-He plasma

Momentum equation: $\nabla \cdot (\rho \vec{v}\vec{v}) = -\nabla p + \nabla \cdot (\mu \nabla \vec{v}) + \rho \vec{g}$

Continuity equation: $\nabla \cdot (\rho \vec{v}) = 0$

Neutral transport equation: $\nabla \cdot (\rho c_C \vec{v}) = \nabla (D \nabla (\rho c_C)) - S_i$

Ions transport equation: $\nabla \cdot (n_i \vec{v}) = \nabla (D_a \nabla n_i + D_{th\,diff} \nabla T + D_{th\,diff,e} \nabla T_e + j_e \gamma_{e,i}) + S_i, \qquad S_i = \alpha n_e n_{C,Ar} - \beta n_e^3$

Transport of electrons: $\vec{E} = \nabla V = -\frac{k}{e}(1 + C_e^{(e)}) \nabla T_e - \frac{k}{e} T_e \nabla \ln n_e + \frac{\vec{j}_e}{\sigma}$

Equation of state: $p = (n_{neutrals} + n_i) kT + n_e k T_e$

Energy balance of electrons: $\nabla \cdot \left((2.5 + A_e) k T_e \frac{\vec{j}_e}{e} \right) = \nabla \cdot (\lambda_e \nabla T_e) - S_i E_i - Q^{electrons-heavy} - Q^{rad} + \vec{j} \cdot \vec{E}$

Energy balance of heavy particles: $\nabla \cdot (\rho \varepsilon \vec{v}) = \nabla \cdot (\lambda \nabla (T)) + Q^{electrons-heavy} + \vec{j}_i \cdot \vec{E}$

Quasi neutrality: $n_e = n_i$

$Q^{electrons-heavy}, \sigma, \lambda_e$ *are functions of* $(T_e, T, n_e, n_a, Q_{e,i}, Q_{e,a})$

$Q^{rad} = f(T_e, p)$

2D setup: boundary and interfacial conditions

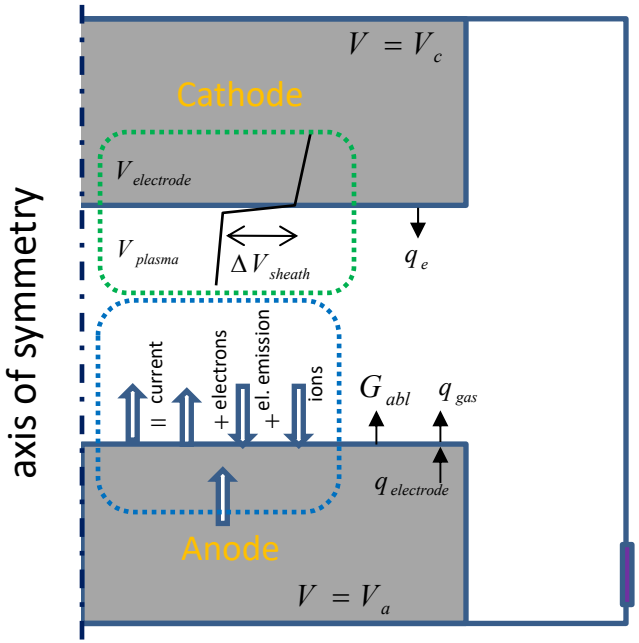

Plasma-electrode interfaces:

Ablation-deposition:

$$G_{abl} = \left(p_{satur,k}(T) - p_k\right)\sqrt{M_c/(2\pi RT)} \quad p_k = n_k kT$$

Electric current and potential:

$$V_{solid} = V_{plasma} + \Delta V_{sh}$$

$$j_{n,plasma} = j_e^{emission} - j_e^{plasma\ to\ electrode} + j_i = f(\Delta V_{sh}, T, T_e, n_e)$$

Heat fluxes include processes: ablation and deposition, emission, radiation, sheath, work function, ionization.

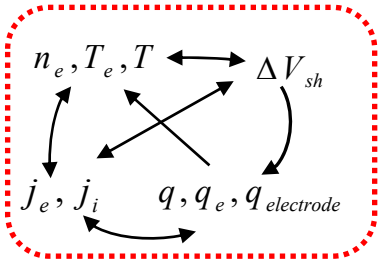

Very nonlinear self-consisted model with many parameters coupled at electrodes:

The current density is non-uniform at the electrode surfaces.

Benchmarking of the model, 1D simulations

Argon arc, near-cathode layer: nonequilibrium region, effects of boundary conditions

our code, simulations by N. Almeida *et al.* **A. Khrabry *et al*, Phys. Plasmas 25, 013521 (2018)**

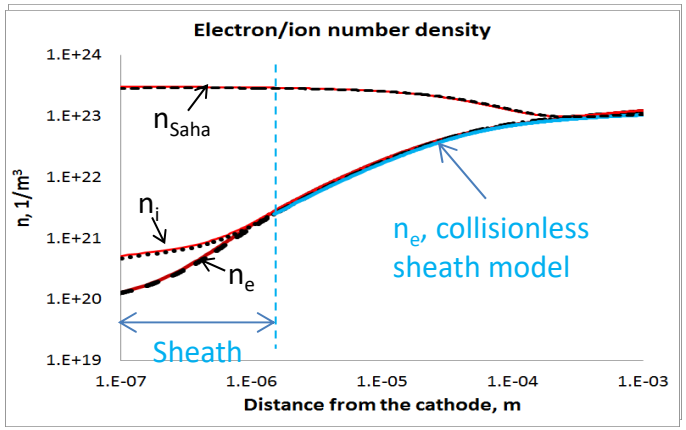

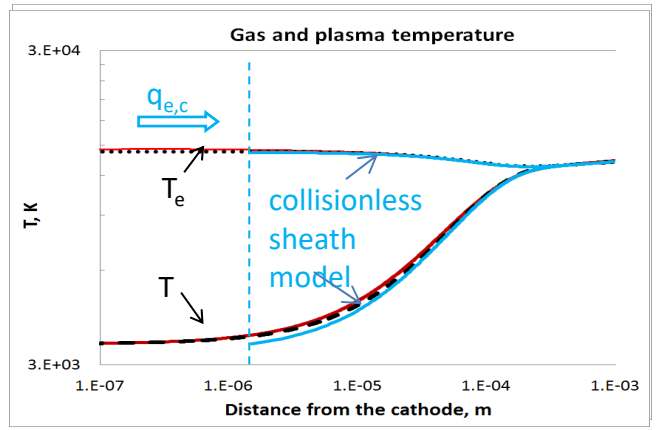

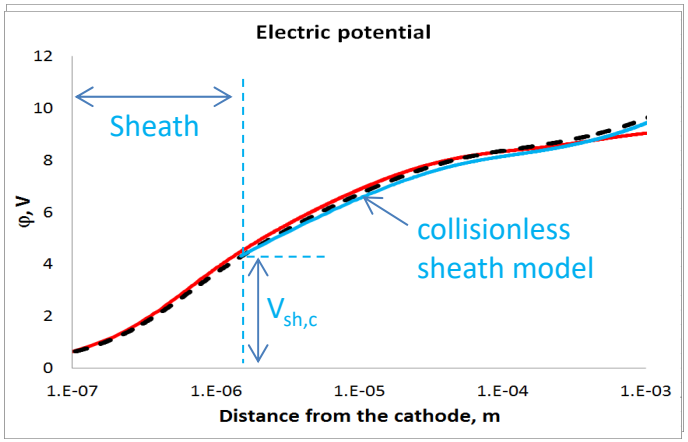

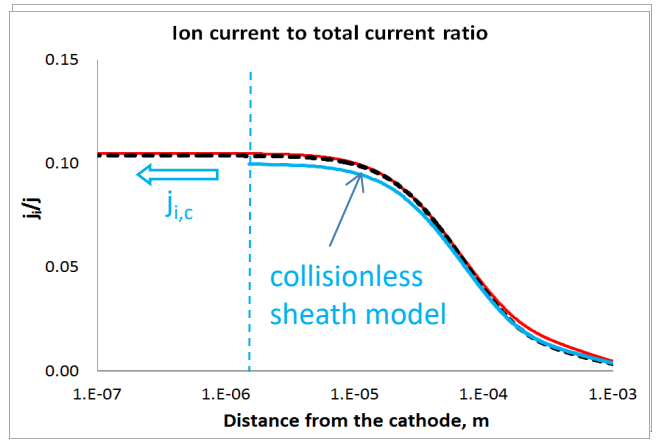

P = 1 atm

$j = 5\cdot10^6$ A/m²

$T_{cathode}$ = 3500K

Collisionless sheath model:

$$j = j_{e,c}^{p} + j_{e,c}^{emiss} + j_{i,c}$$

$$j_{i,c} = q_e n_i \sqrt{\frac{k(T_e + T)}{m_a}}$$

$$j_{e,c}^{p} = q_e n_e \frac{1}{4}\sqrt{\frac{kT_e}{m_e}} \cdot e^{-\frac{V_{sh,c}}{kT_e}}$$

$$q_{e,c} = j_{e,c}^{emiss}\left(V_{sh,c} + 2.5T_c\right) - j_{e,c}^{p}\left(V_{sh,c} + 2.5T_e\right)$$

Self-consistent current density profile

Simulations:

Electric current streamlines:

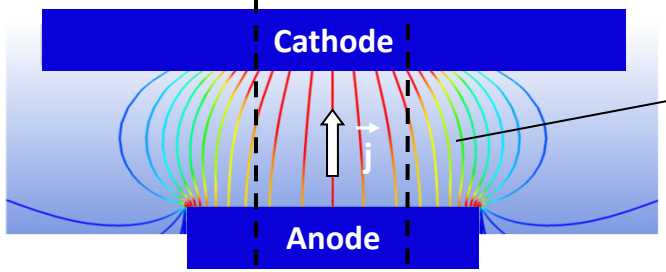

Electric potential profile:

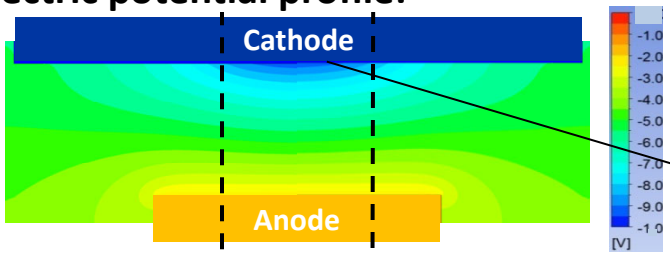

Non-uniform potential profile along the cathode.

Experiments with a segmented cathode:

Y.-W. Yeh et.al., Carbon 2016

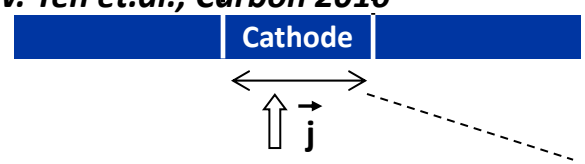

2 radial segments, central segment d=3.2mm, 95% of current

Simulations: 75% of current flows through 3.2mm segment

V. Vekselman, et al., PSST 27, 025008 (2018)

Arc channel

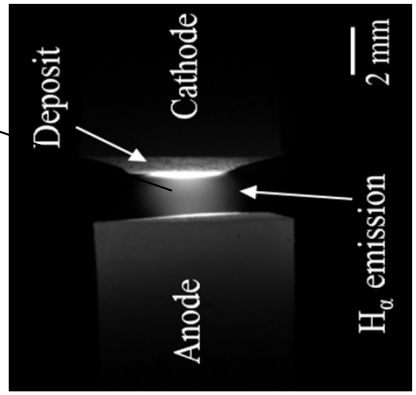

Middle plane plasma density profile:

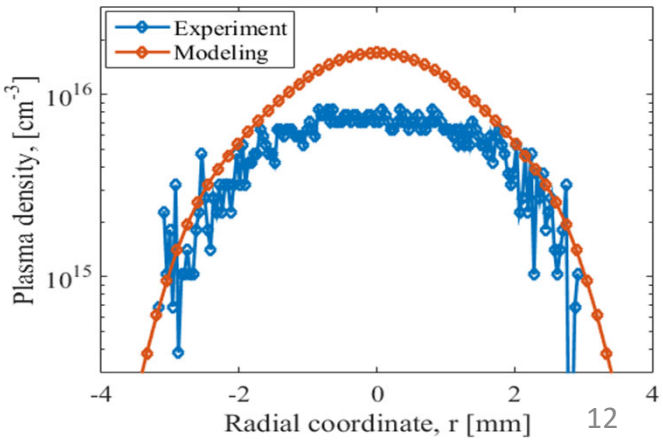

Towards predictive modeling of atmospheric plasma for synthesis of nanomaterials

- **Plasma density obtained from H_α OES and 2-D CFD simulations**

Arc operation: Current 55 A, He pressure 500 torr

Inhomogeneity of the arc plasma is due to narrow arc channel

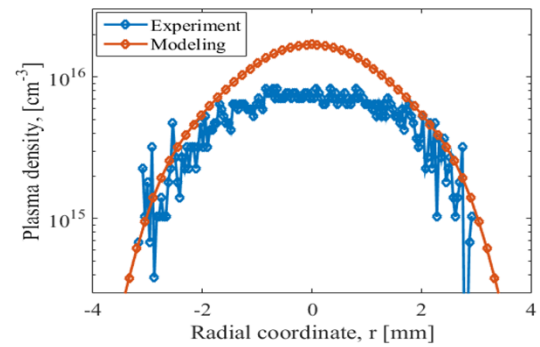

- **C_2 density obtained from LIF (a) and 2-D CFD (b)**

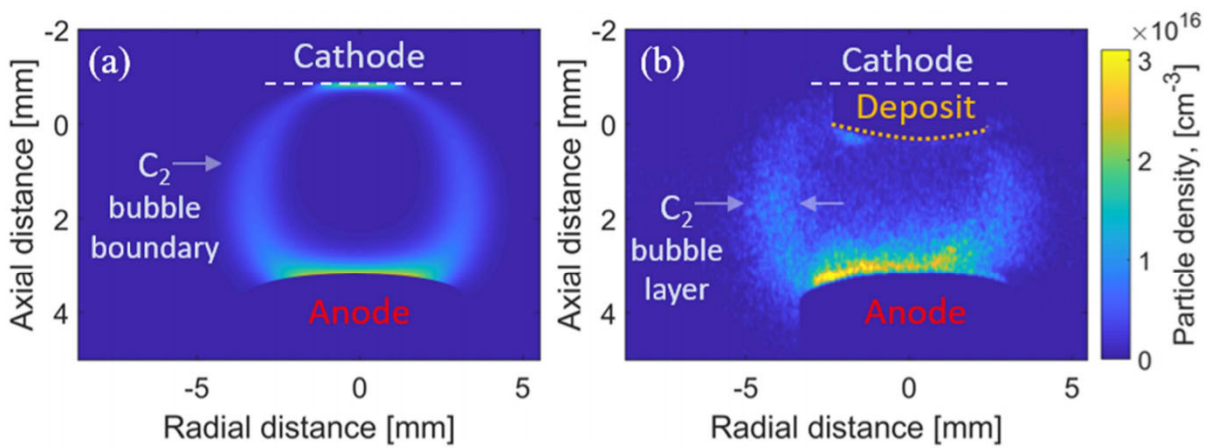

Figure 4. Comparison of (a) simulated and (b) measured C_2 density distribution in the arc at current 50 A. change in the cathode surface topology due to the growth of deposit (b) was not accounted for in the simulation (a).

Gas flow controls transport of carbon in the arc

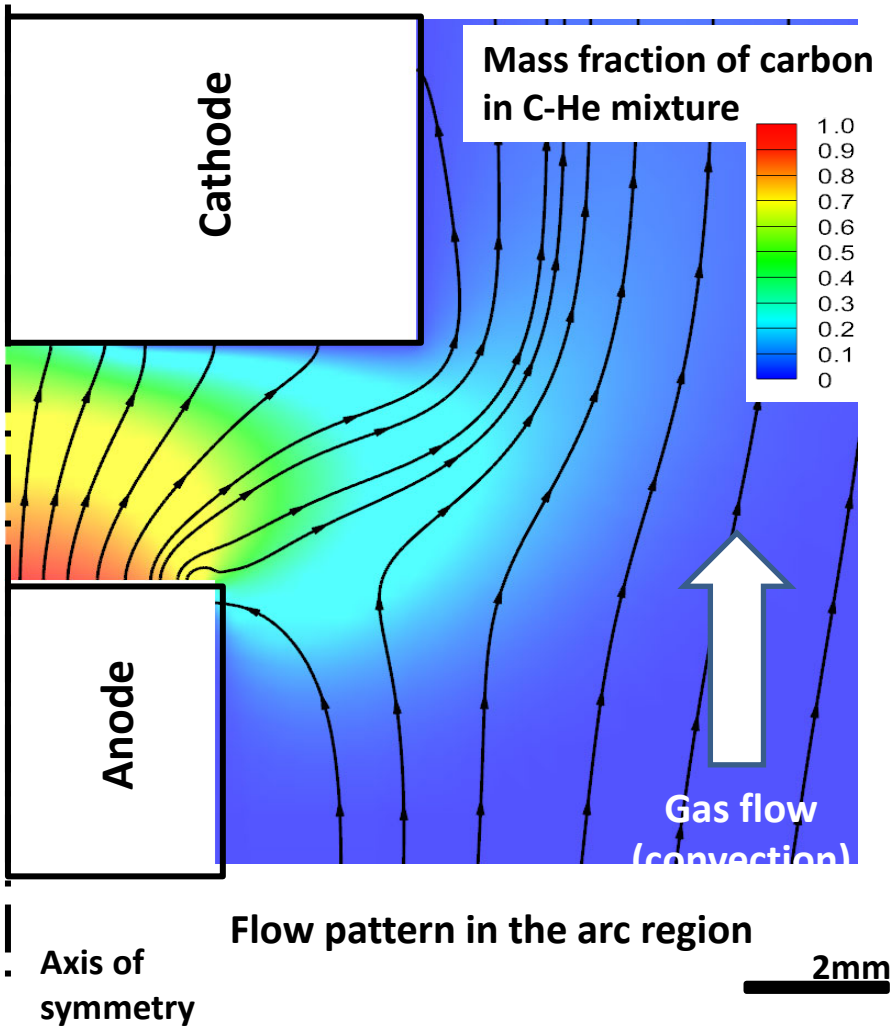

Flow pattern in the arc region

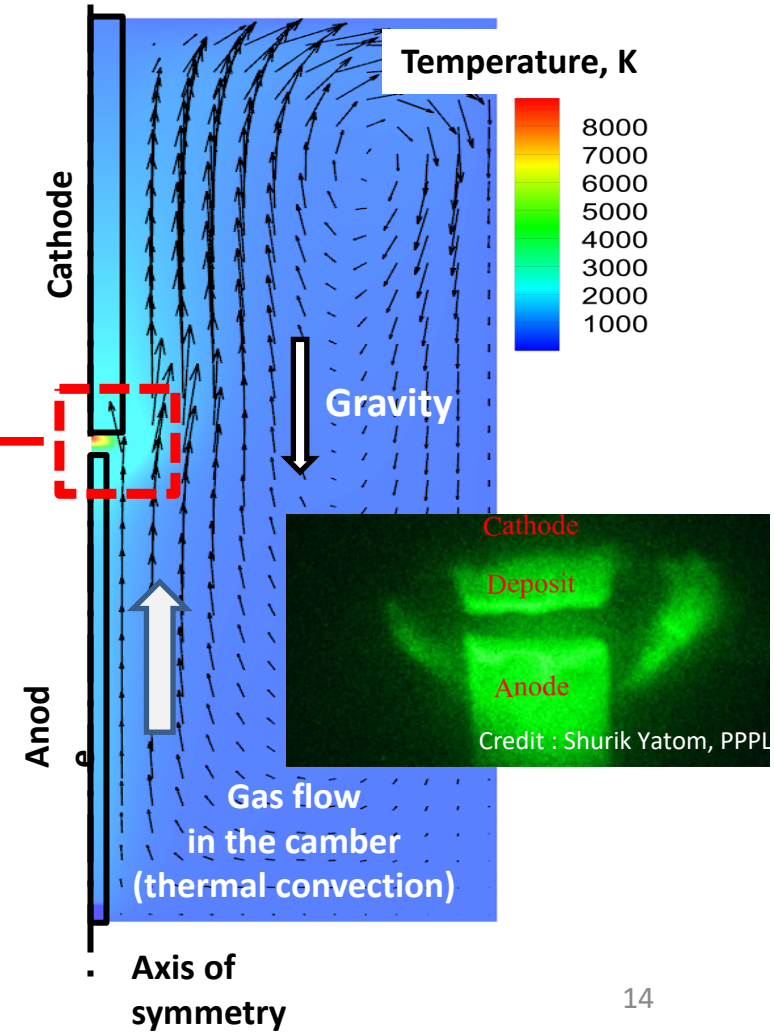

Analytical model of low and high ablation regimes in carbon arcs

- **The ablation rate is a strong nonlinear function of the arc current.**
- **We developed analytical model that explains this transition.**

Fig. Ablation rate of anode as a function of arc current.

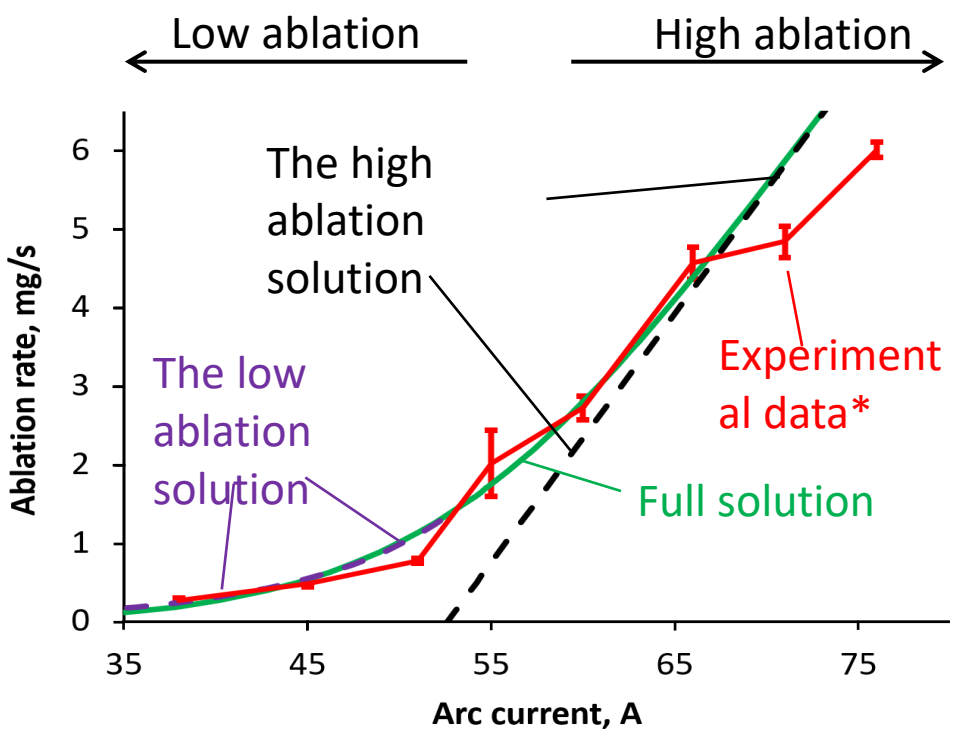

A. Khrabry, et. al., Journal of Applied Physics **128**, 123303 (2020).

Analytical model of low and high ablation regimes in carbon arcs

- **Ablation flux grows drastically with the surface temperature T_a**
- **We developed analytical model for ablation flux g_{abl}**

Fig. Schematics of carbon ablation into He gas.

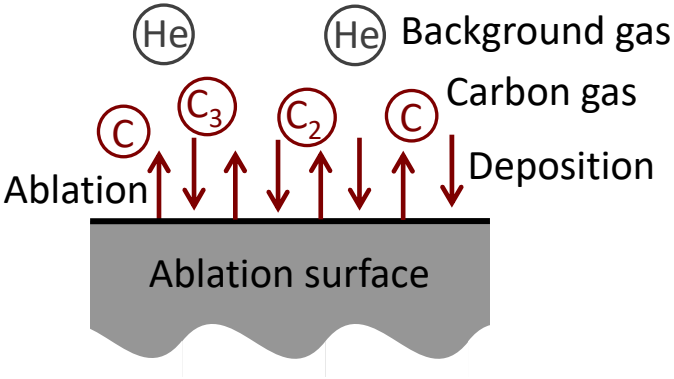

$$g_{abl} = \left(p_{sat,C}(T_a) - p_{C,a}\right)/v_{th}$$

$$g_{abl} = D_{C-He}\frac{dn_C}{dx}$$

Fig. Ablation flux as a function of surface temperature.

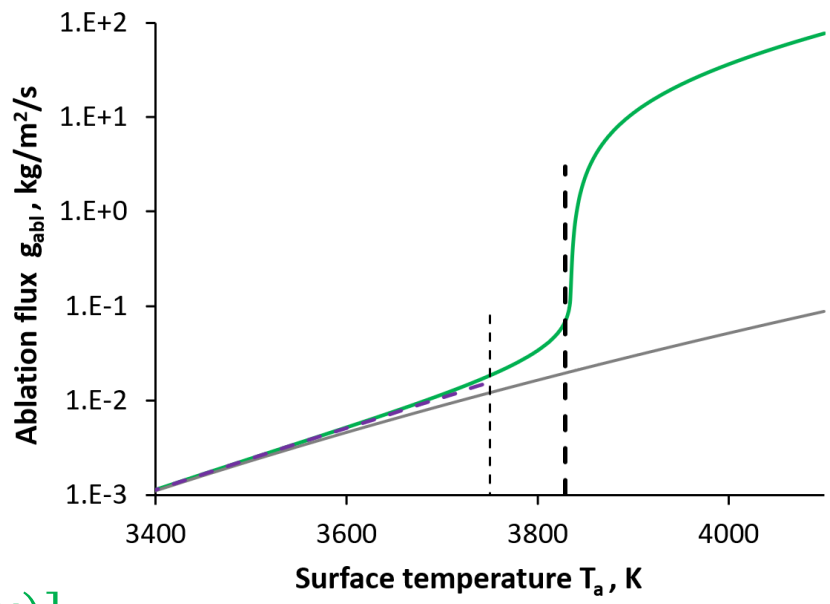

$$g_{abl}v_{th}(T_a) = p_{sat,C}(T_a) - p_0\left[1 - \exp\left(-\frac{g_{abl}}{g_0}\right)\right]$$

Analytical model of low and high ablation regimes in laser ablated graphite

Fig. Schematics of laser experiment.

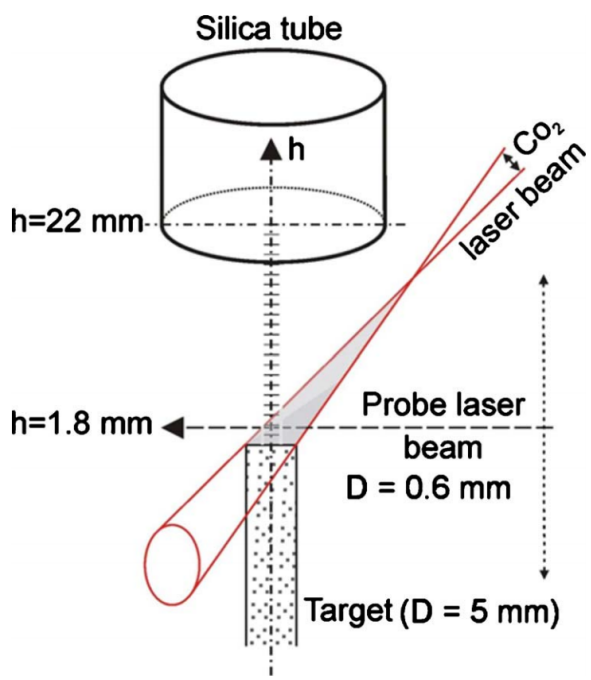

M. Cau et. al., Physical Review B **81**, 165416 (2010)

Fig. Ablation flux as a function of 1/(surface temperature).

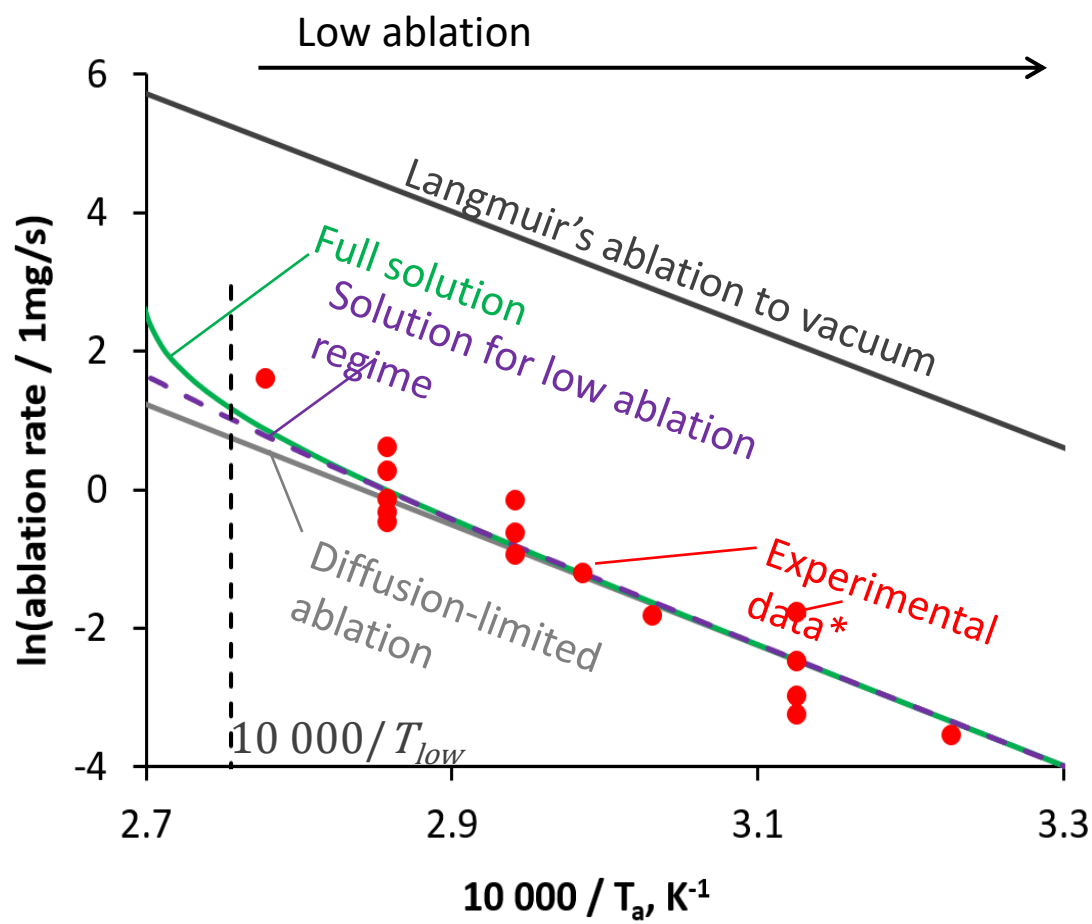

Ablation rate as a function of arc current can be determined from the energy balance

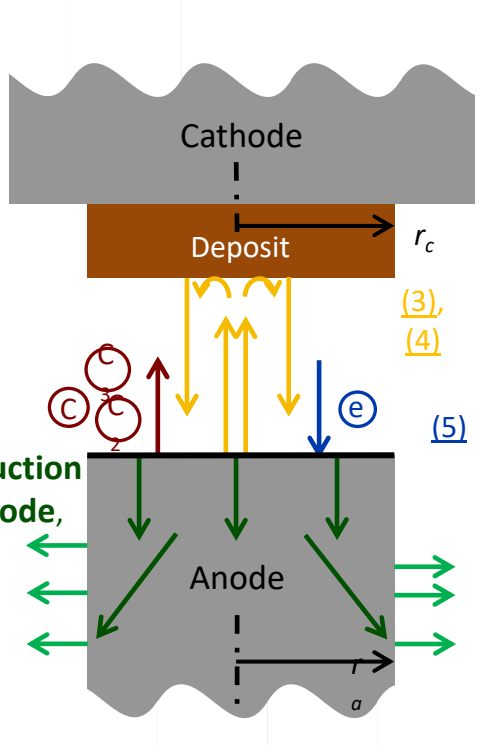

(1) **Ablation** (latent heat)

(2) **Heat conduction into the anode**, with further radiation from its sides

(3), (4) **Radiation from front surfaces**

(5) **Electron heat flux** :
- thermal energy
- work function
- sheath voltage

Sum of heat sinks = sum of heat sources

(1) + (2) + (3) = (4) + (5)

$$\pi r_a^2 g_{abl}(T_a) L + C_1 T_a^{2.5} r_a^{1.5} + C_2 r_a^2 T_a^4 = C_3 r_a^2 + V_{eff}\, I$$

$$V_{eff} = V_w + 2.5\frac{k}{e}T_{e,a} + \max(V_{sh}, 0) = 9.5V$$

$$C_1 = \pi\sqrt{\frac{4}{5}\sigma\varepsilon_a\lambda_a}$$

$$C_2 = \pi\sigma\varepsilon_a(1-\alpha_r)$$

$$C_3 = \pi\sigma\varepsilon_a\varepsilon_c F_{c-a} T_c^4$$

A. Khrabry, et. al., *Journal of Applied Physics* ***128***, *123303 (2020)*

The ablation rate as function of arc current is in a good agreement with experimental data.

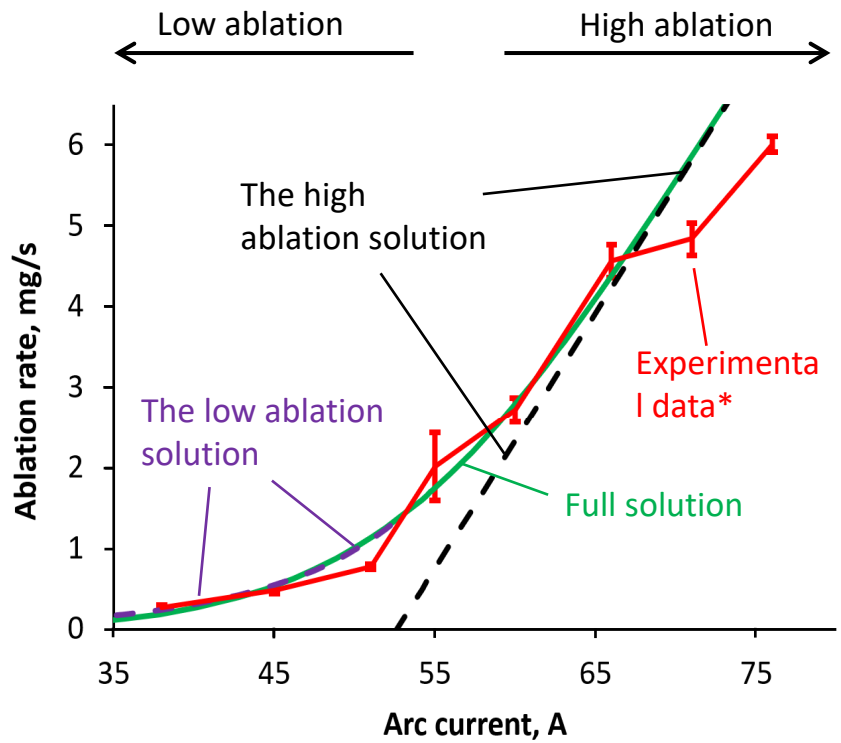

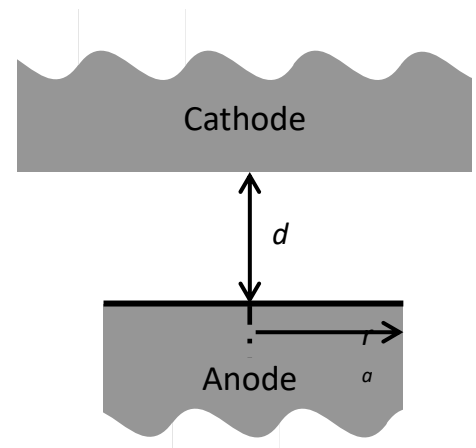

r_a = 3 mm **d = 1.5 mm** **p = 67 kPa (500 Torr)**

Variable arc current

V. Vekselman et.al., Plasma Sources Sci. Technol. **26, 065019 (2017)*

A. Khrabry, et. al., *Journal of Applied Physics **128**, 123303 (2020)*

The ablation rate as function of anode radius is in a good agreement with experimental data.

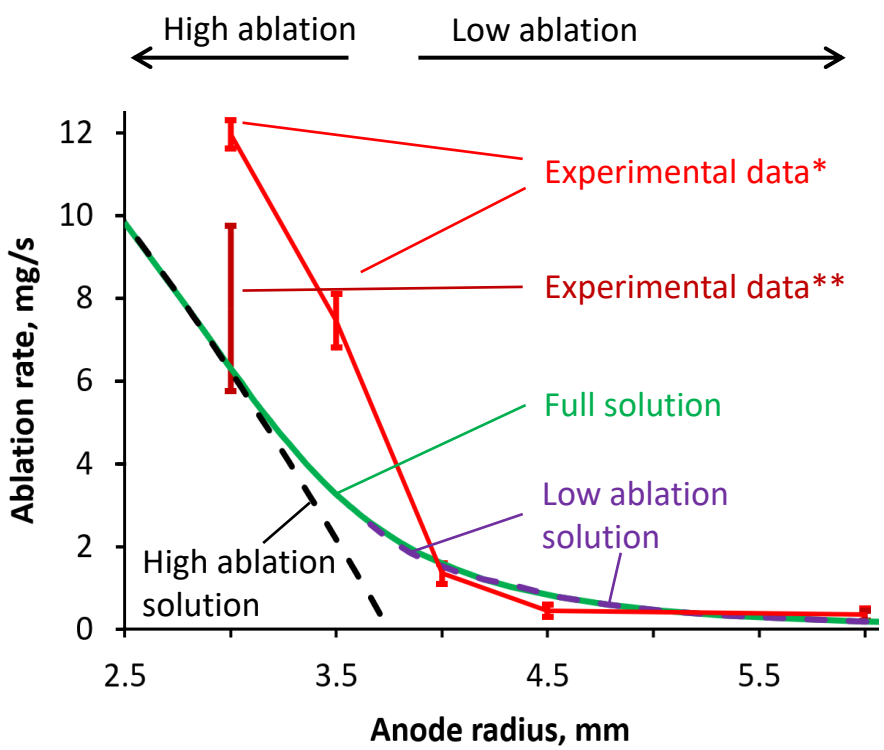

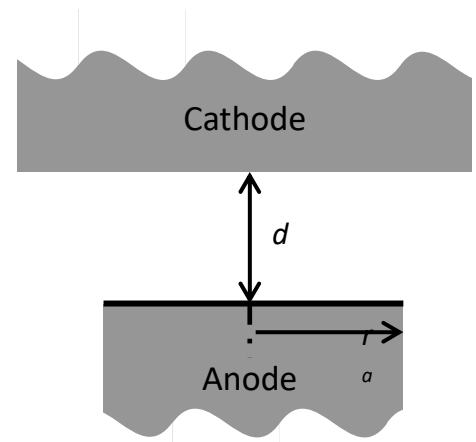

I = 65 A **d = 1.5 mm** **p = 67 kPa (500 Torr)**

Variable anode radius r_a

** J. Ng and Y. Raitses, J. Appl. Phys. **117**, 063303 (2015)*

*** J. Ng and Y. Raitses, Carbon **77**, 80 (2014)*

A. Khrabry, et. al., *Journal of Applied Physics **128**, 123303 (2020)*

The ablation rate as a function of inter-electrode-gap width is in a good agreement with experimental data.

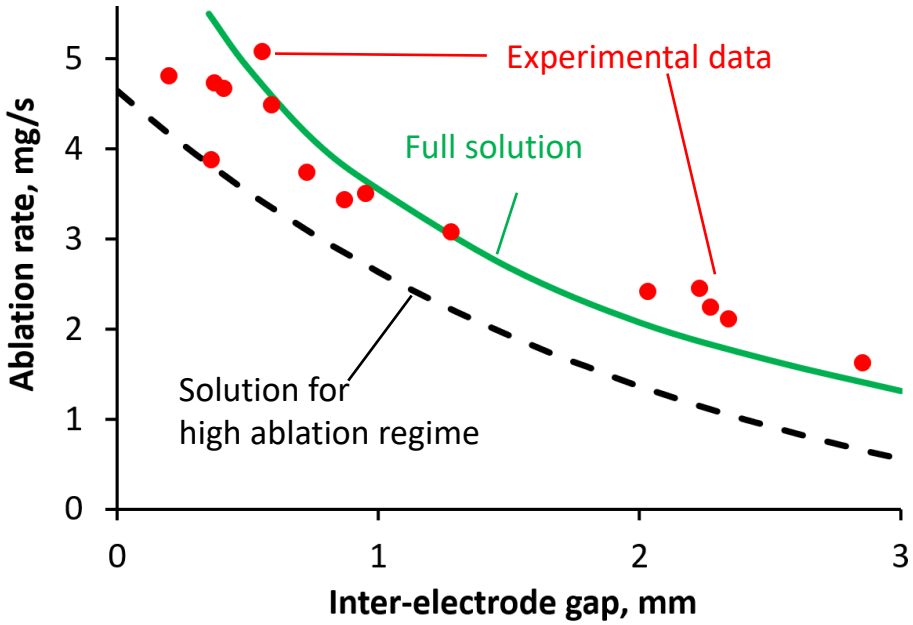

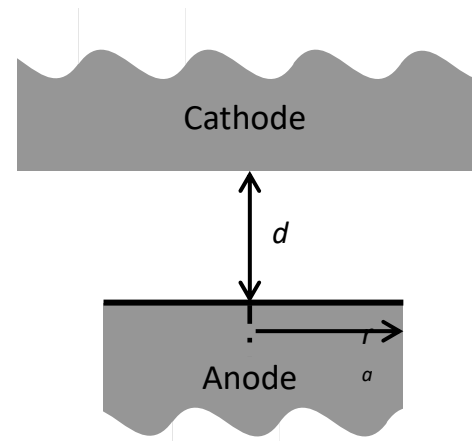

I = 60 A **r_a = 3 mm** **p = 67 kPa (500 Torr)**

Variable electrode separation distance

A. Khrabry, et. al., *Journal of Applied Physics* ***128****, 123303 (2020)*

The ablation rate curves as function of current shift towards higher arc currents with the background pressure increase proving diffusion limited regime

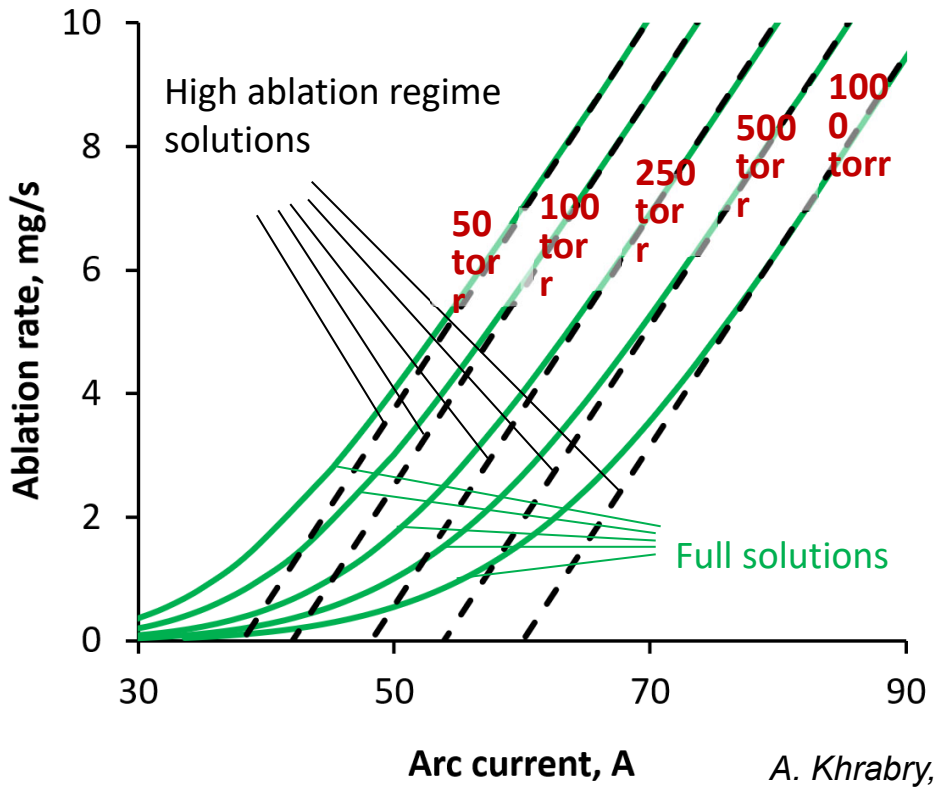

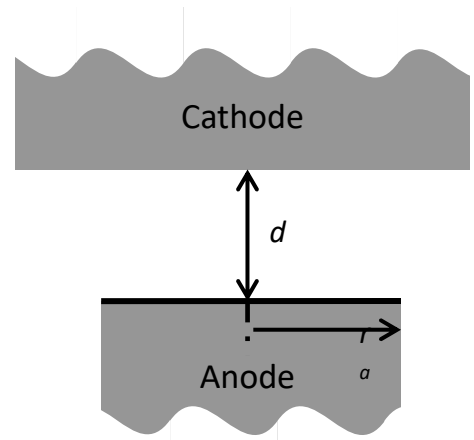

r_a = 3mm d = 1.5 mm

Variable arc current and pressure

A. Khrabry, et. al., *Journal of Applied Physics* ***128****, 123303 (2020)*

Arc anode spot formation observed and explained

Current density profiles on anode front surface

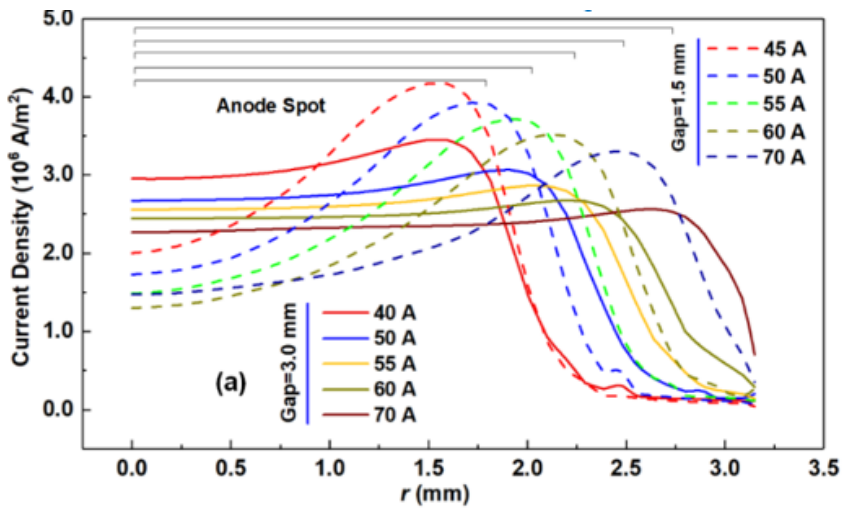

Surface temperature profiles on anode front surface

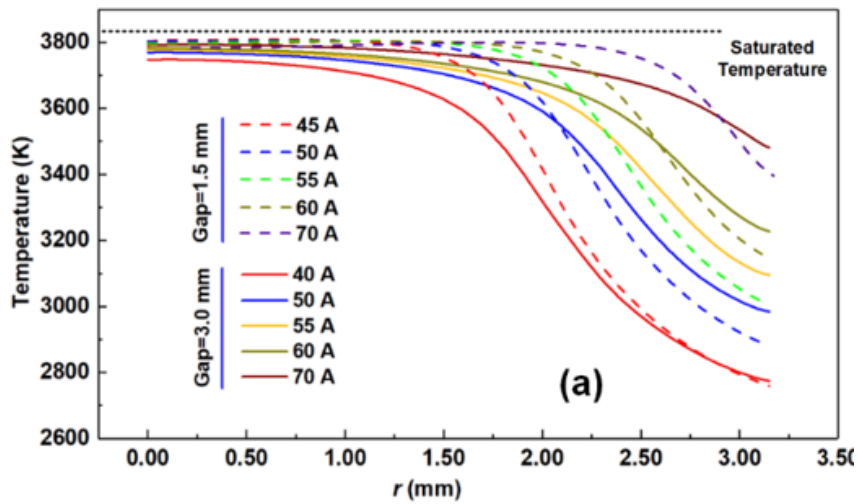

Experimental observation of anode spot in PPPL setup

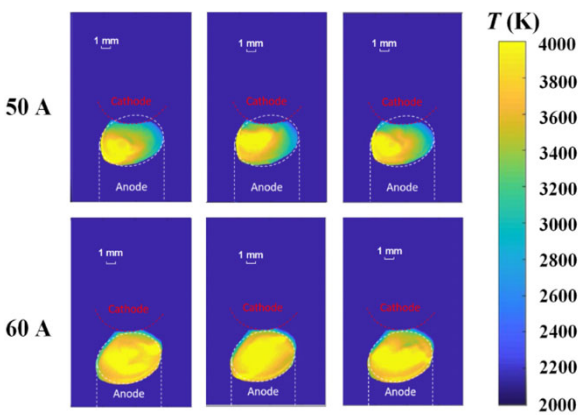

Characteristics observed in both simulations and experiments:

- **Spot size increases with arc current**
- **Temperature inside the spot is relatively uniform and is about the carbon evaporation temperature.**

J. Chen, et *al*, PoP 27, 083511 (2020)

Analytical model of arc anode spot formation

Schematic of the reduced model

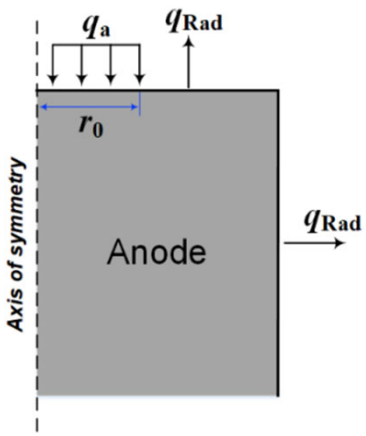

Comparison of anode radii obtained in the full simulations, reduced model and experimental data

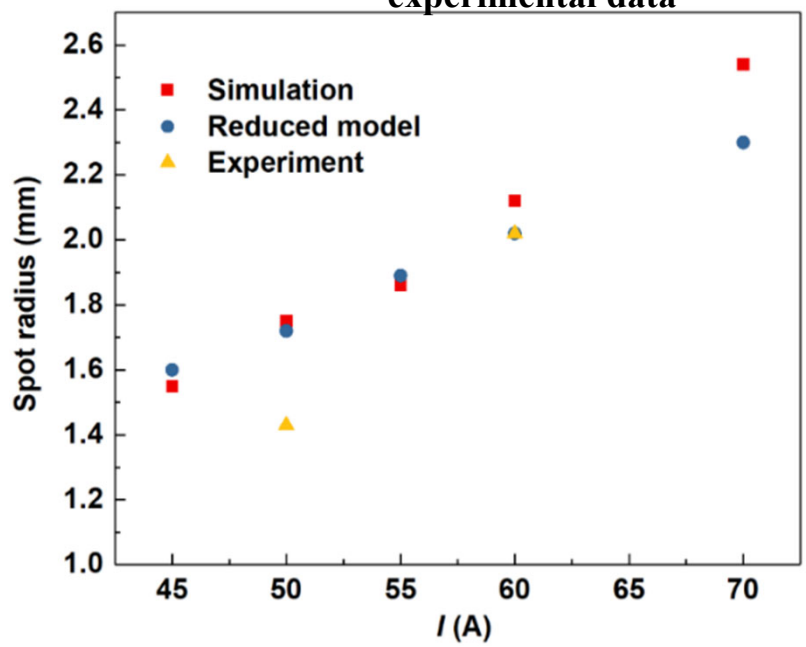

Problem can be reduced to a cylindrical heat conduction problem in the anode:

The net heat flux from plasma are balanced by heat loss from its surface through heat conduction. Nonlinear processes in ablation and radiation give a unique nonuniform solution for the anode spot.

J. Chen, et *al.*, PoP 27, 083511 (2020)

Outline

nano.pppl.gov

- **Modeling of nanoparticle nucleation and growth**

Measurements and simulations of nanoparticles

Experimental set up for laser-induced incandesce (LII), spectral imaging, and the laser beam intersection with the region of nanoparticle growth.

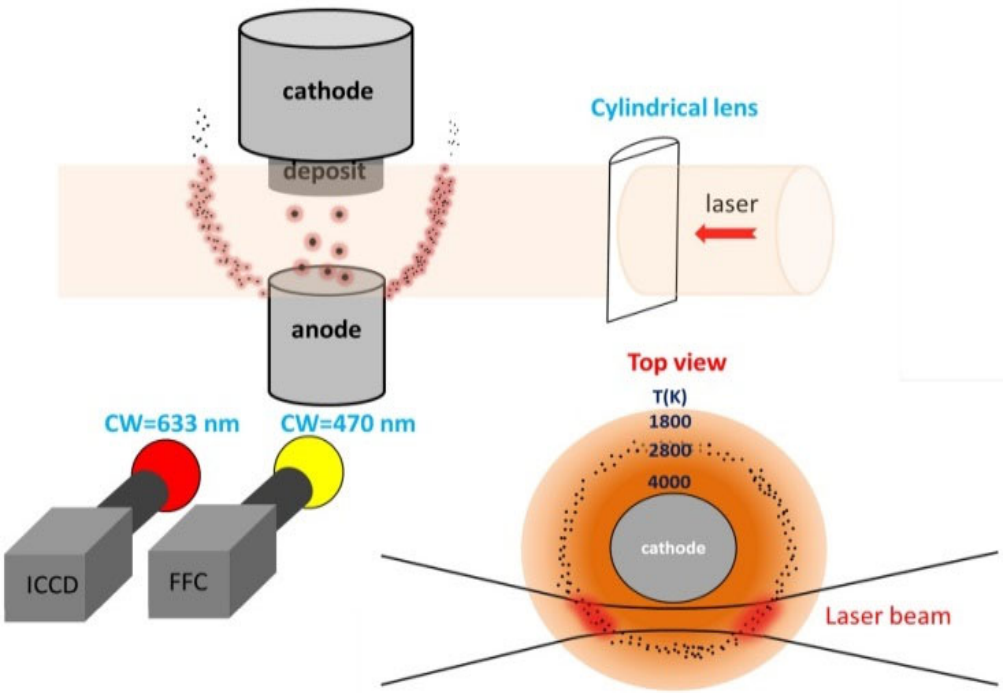

Areas from which a LII signal was collected are highlighted and the mean particle diameter for each area is shown from LII (yellow) and simulations (white). S. Yatom, et al, MRS (Material Research Society) Communications (2018).

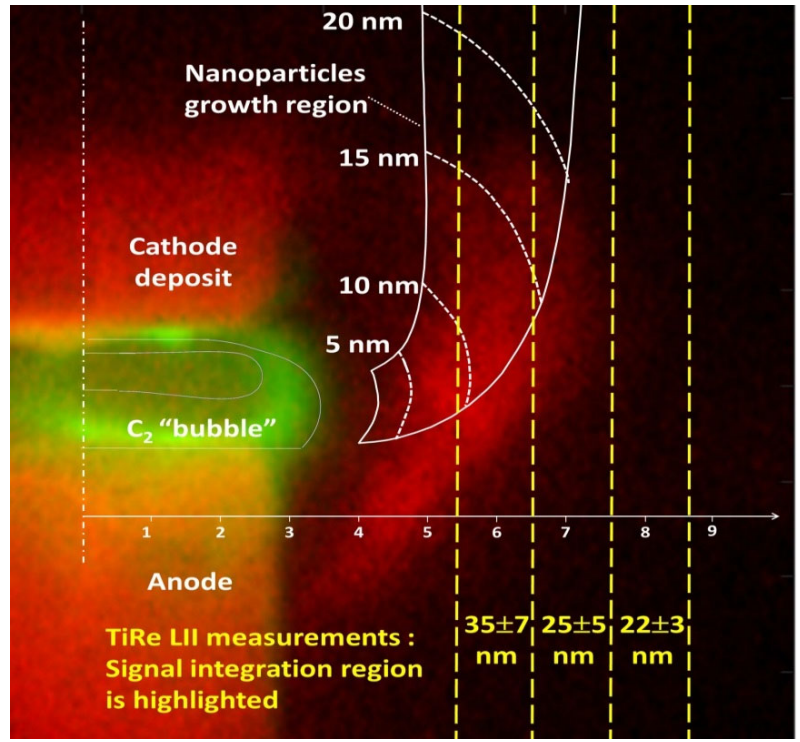

An Analytic Expression for Cluster Mean Diameter and Dispersion After Nucleation Burst Measurements

Modeling of nucleation burst is very complicated because it involves solving for very complex nonlinear nucleation rate.
Using an approximation for nucleation rate and Frielander's momentum model for cluster distributions we derived formulas for cluster mean diameter and dispersion.

Fig. Mean diameter after nucleation as a function of the cooling rate normalized on $\dot{T}^*_0$=1000K/s, analytic formula (crosses) Friedlander's model (lines) for two ambient gas pressures. ΔT is the temperature change after nucleation burst.

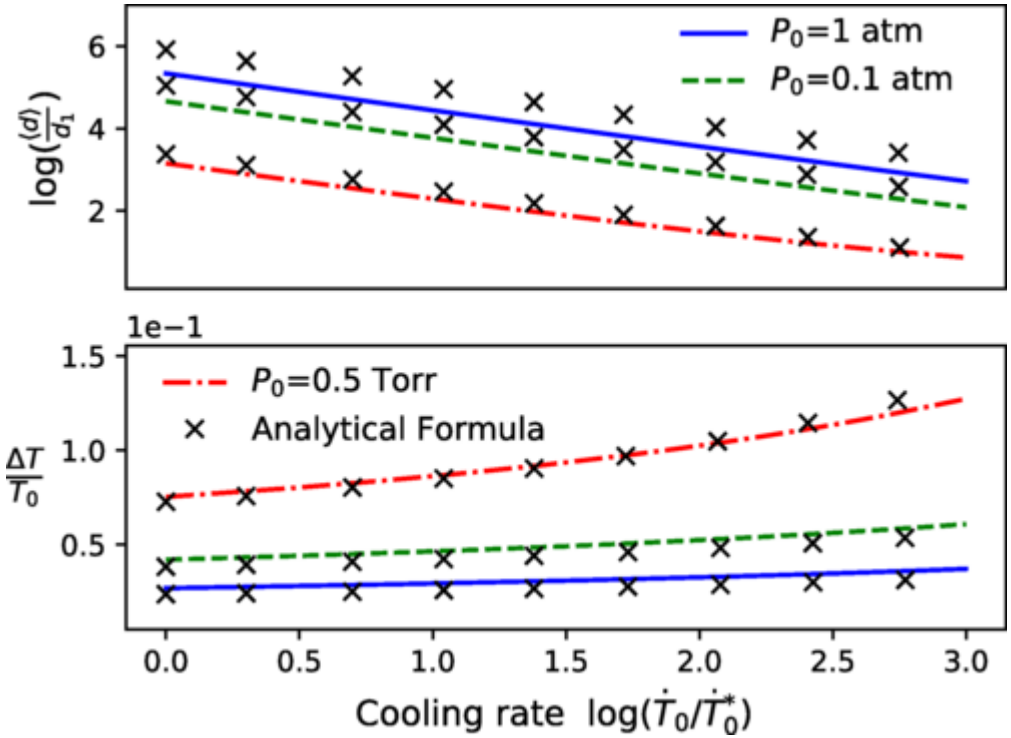

M. Tacu, A. Khrabry, and I. D. Kaganovich, Phys. Rev. E **102**, 022116 (2020)

Outline

nano.pppl.gov

- **Atomistic simulations of key processes of nanotube growth**
  - **Carbon nanomaterials**

Charging of nanotubes affects adatom absorption and diffusion

a)

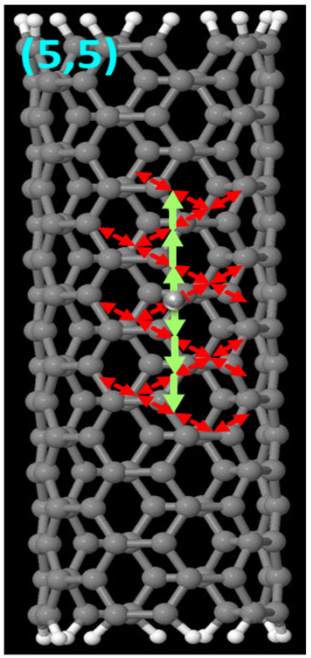

- **Charging of nanoparticles and nanostructures is a plasma effect on nucleation and growth processes**
- **DFT and Kinetic Monte-Carlo simulations of charging effect**
- **Armchair (5,5) SWCNT (Fig. a)**
- **Charging of the CNT causes the higher adsorption energy E_a, increasing the migration distance**

b)

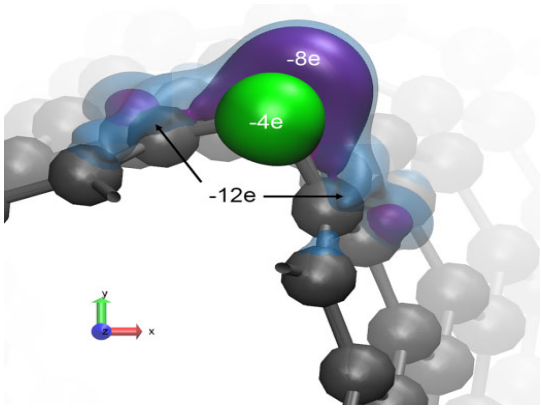

DFT results (Fig. b)- additional charges distribute in the covalent bond space between adatom and CNT, increasing its covalent coupling.

L. Han, P. Krstic, I. Kaganovich, and R. Car, Carbon 116, 174 (2017)

Condensation of carbon gas

- **Simulations by Quantum-Classical Molecular Dynamics with Density Functional Tight Binding Theory**

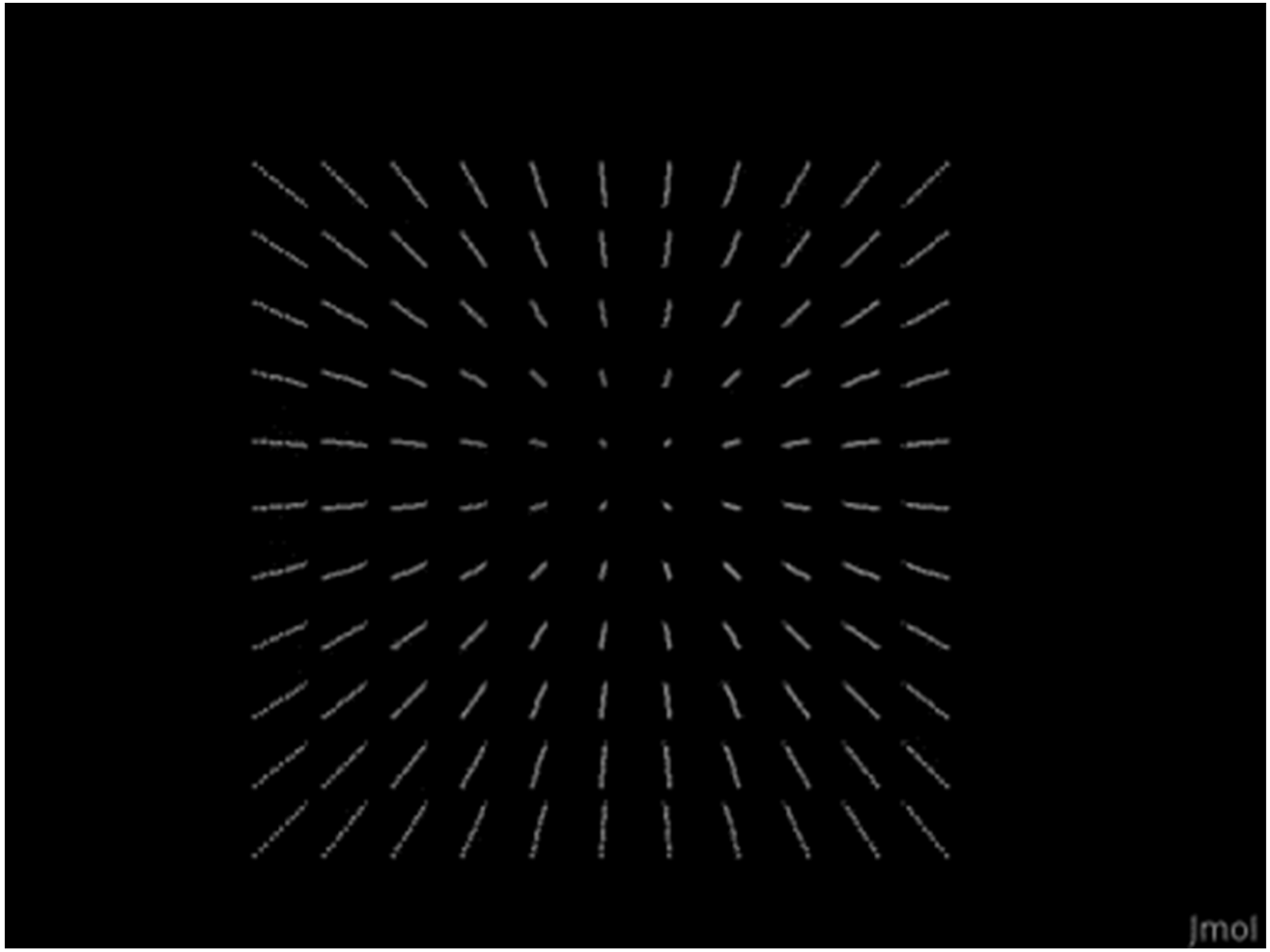

- **Cooling carbon forms chains and fullerenes.**
- **No available carbon vapor for carbon nanotube growth. => Need catalyst for nanotube growth**

L. Han, P. Krstic et al.,

Outline

nano.pppl.gov

- **Atomistic simulations of key processes of nanotube growth**

  - **Boron-Nitride nanomaterials**

Synthesis of Boron Nitride Nano Tubes(BNNT) in arc

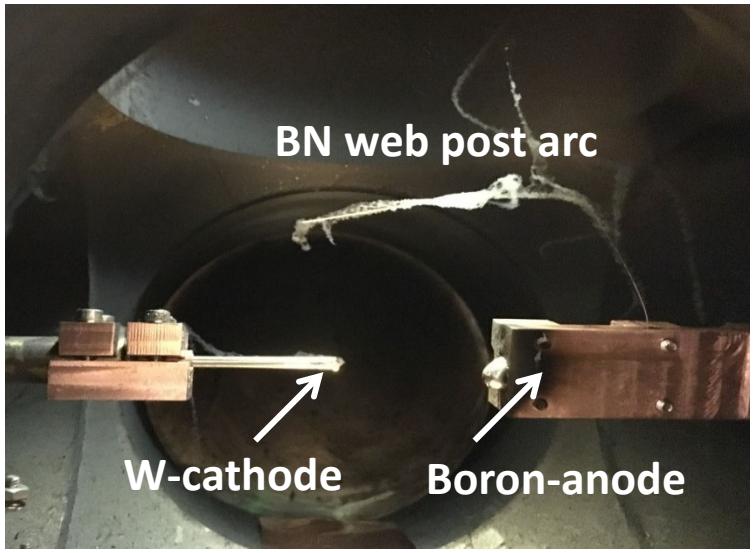

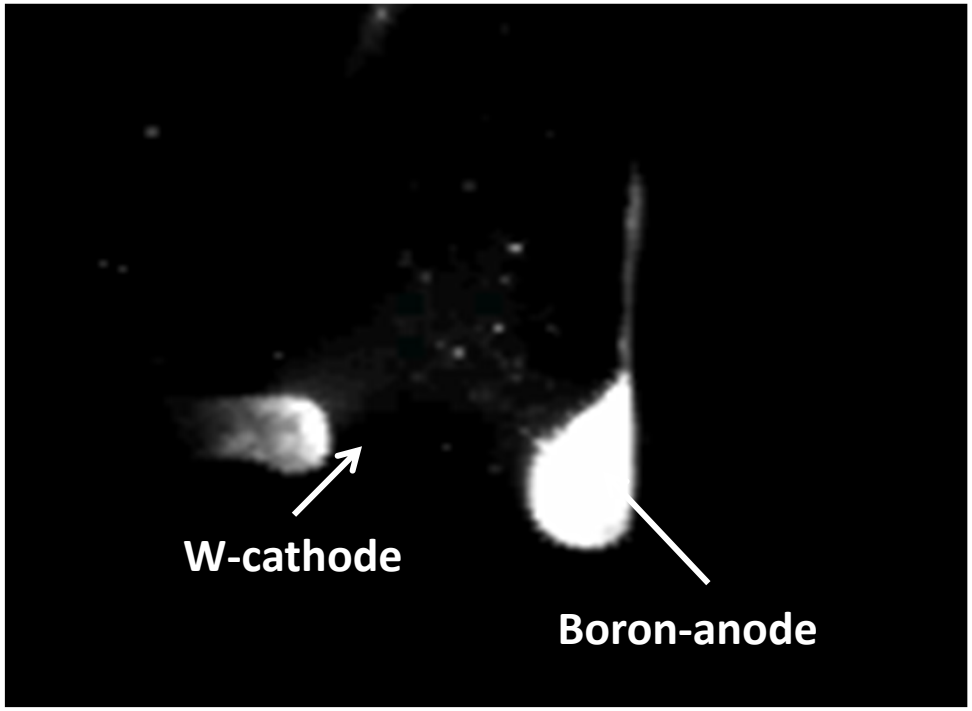

Boron-rich anode and tungsten cathde 40V-40A arc at 400 torr of N_2 (Zettl 2000)

Y. W. Yeh, Y. Raitses, B. E. Koel and N. Yao, **"Stable synthesis of few-layered boron nitride nanotubes by anodic arc discharge",** *Sci. Rep.* ***7****, 3075 (2017).*

Hypothesis of BNNT synthesis

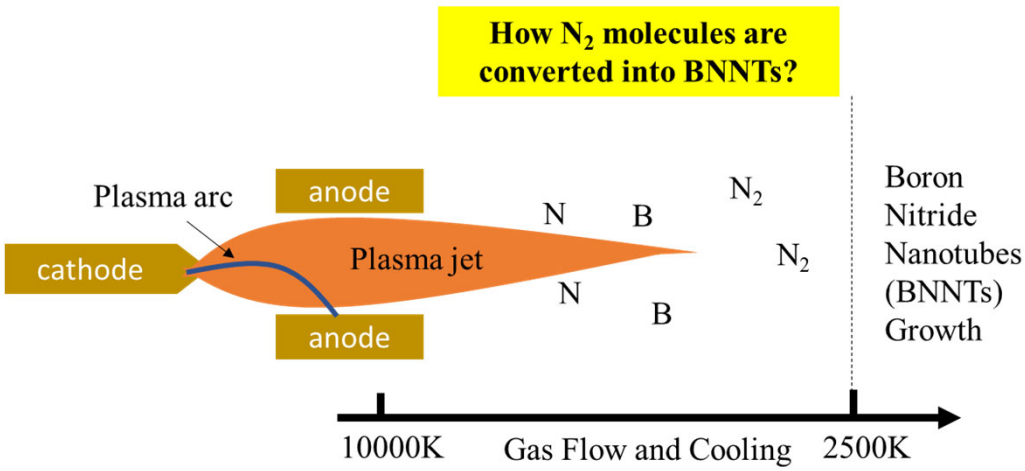

N_2 is dissolved in boron droplets

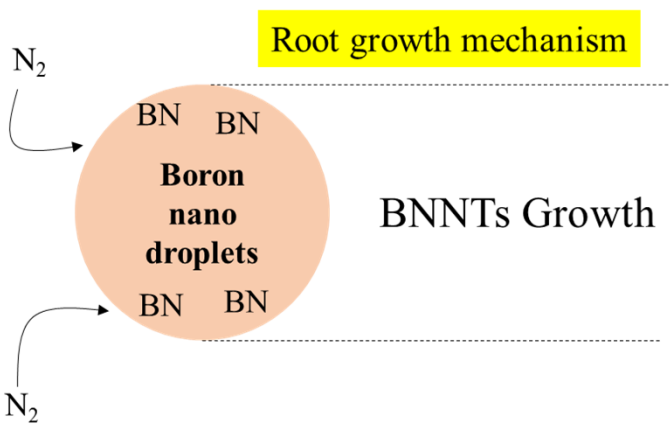

Understanding root growth of BNNT

1. Accumulation of N on the surface of liquid boron
2. Formation of a BN island on the liquid surface
3. Fluctuation and nucleation of a protruding BN cap
4. Growth of the nanotube with root feeding

Order-parameter-driven molecular dynamics DFT simulations predicted formation of a BN cap at 2500 K, B. Santra Nanoscale 10, 22223 (2018).

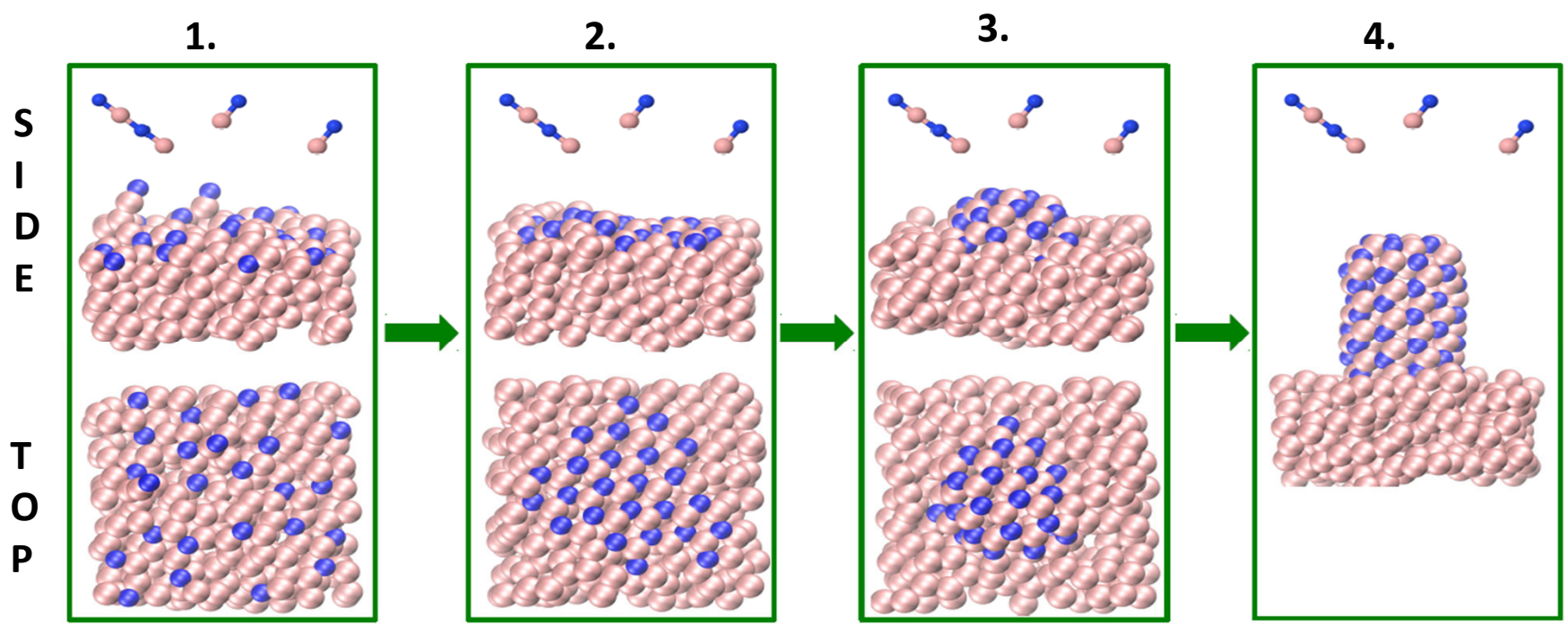

Where BN radicals can come from?

Simulations show that N_2 is not easily dissolved in boron droplets. What else?

There a large barrier to form stable NBN from B+N_2 $B + N_2 \longrightarrow BNN \longrightarrow NBN$

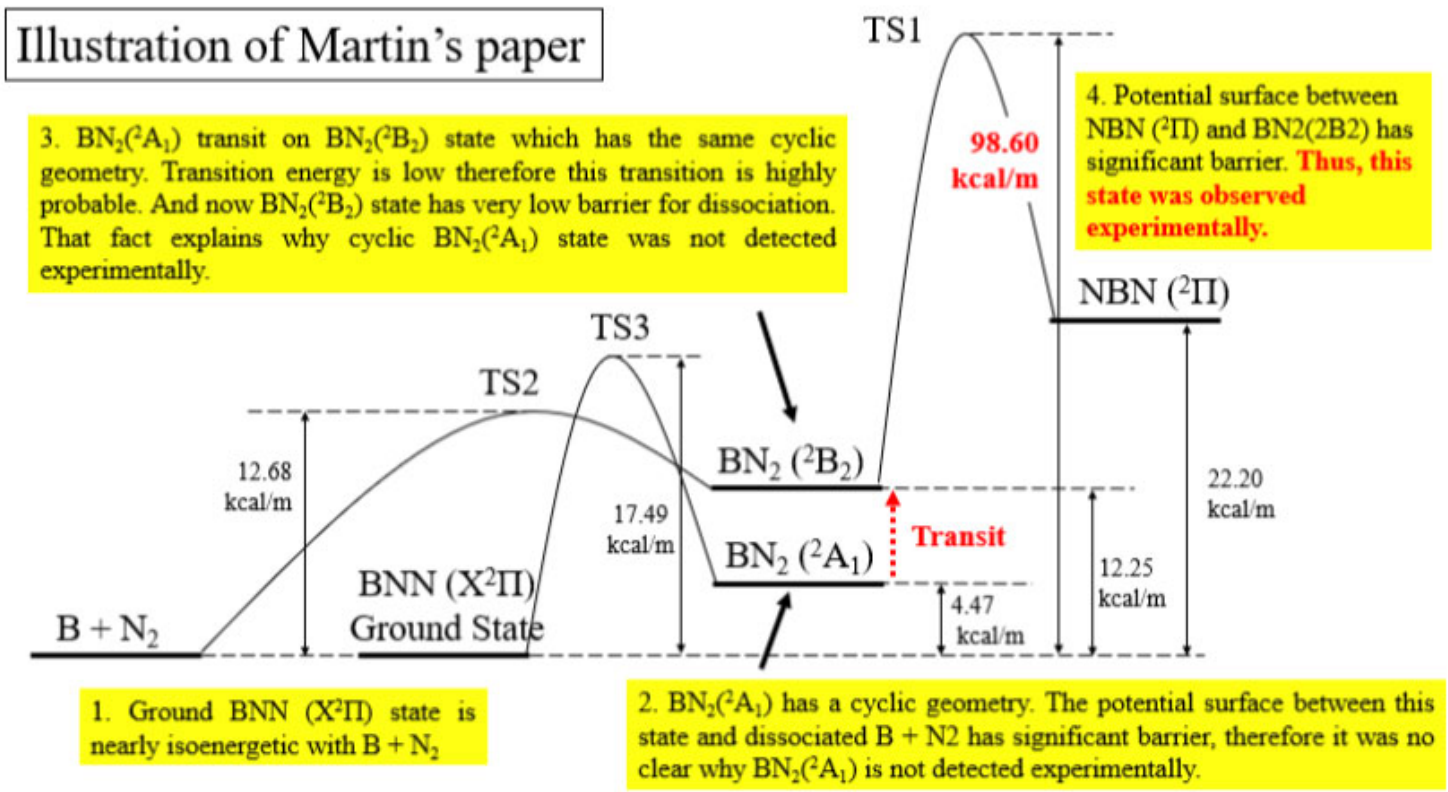

References

"Ab initio study of the spectroscopy, kinetics, and thermochemistry of the BN2 molecule". Martin JML, Taylor PR, François JP, Gijbels R, Chemical physics letters 222, 517 (1994).

1eV = 23.061 kcal/mol

DFT can only simulate the species with the lowest energy for multiple species with the same geometry. This prevents DFT from predicting mechanisms involving other species with the same geometry but higher energy level.

Restrictions of DFT

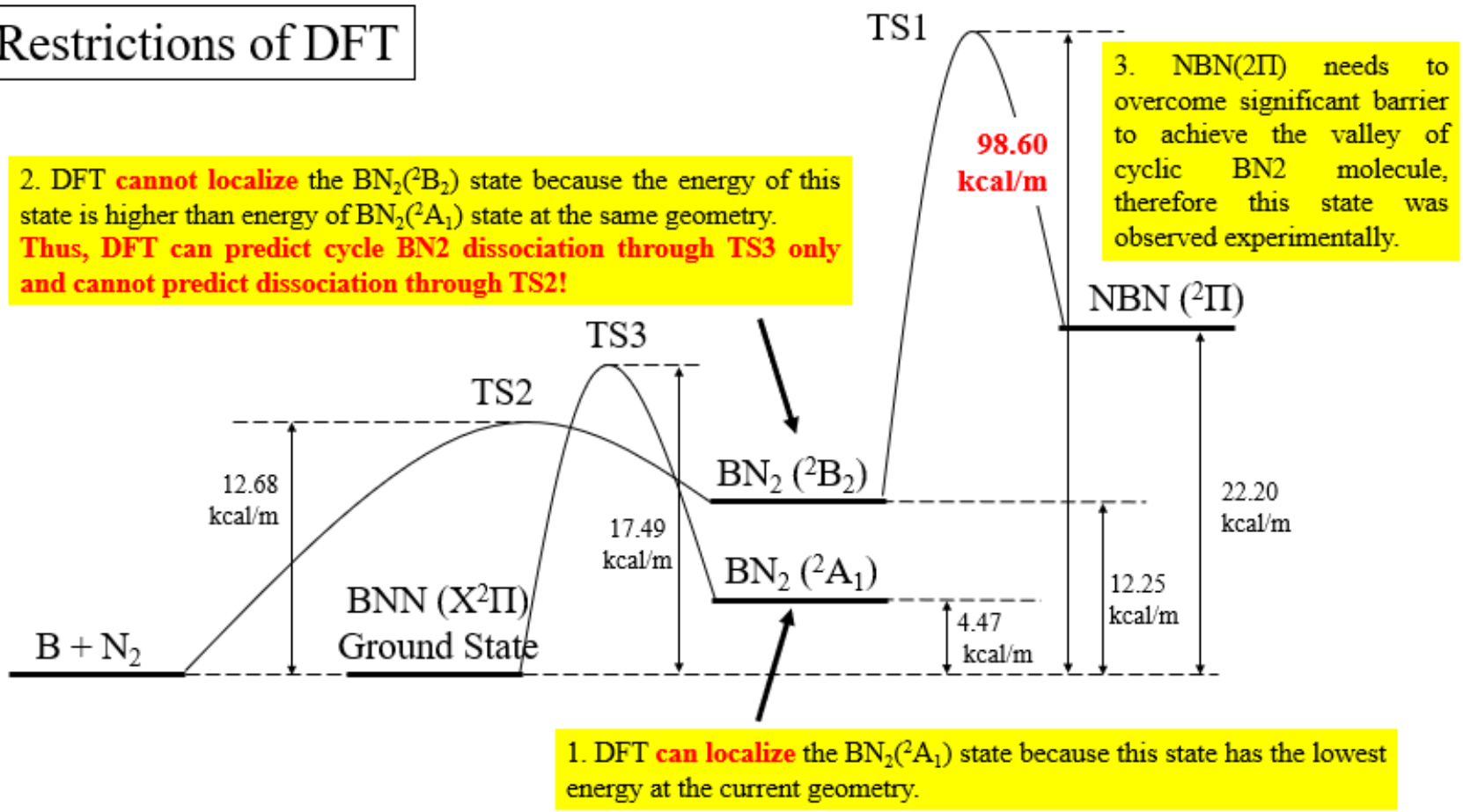

Where BN radicals can come from?

Simulations show that N_2 is not easily dissolved in boron droplets. What else?

We proposed Mechanism for BNBN formation through a Boron dimer and a Nitrogen Dimer. O. Dwivedi et *al.* (2019)

$$B_2 + N_2 \longrightarrow BBN_2 \longrightarrow B_2N_2 \longrightarrow BNBN$$

$B_2 + N_2$ → BNBN Quantum chemistry modeling by Y. Barsukov et *al.* (2020)

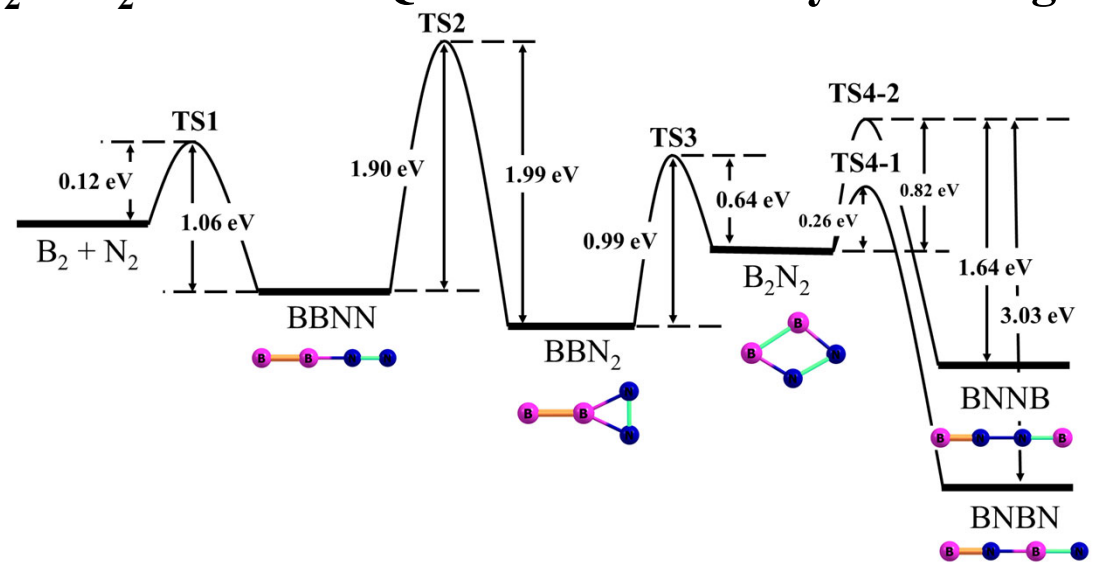

BBNN and BNBN species were detected earlier, L. Andrews et al., J. Chem. Phys., **98**, (1993).

BNBN Formation

Movie. *A) Formation of BNBN from NBN molecule. B) Formation of BNBN from two Boron atoms and a Nitrogen Dimer.* ***O.*** **Dwivedi et *al.* (2019)**

BNBN formation is observed through DFTB+.

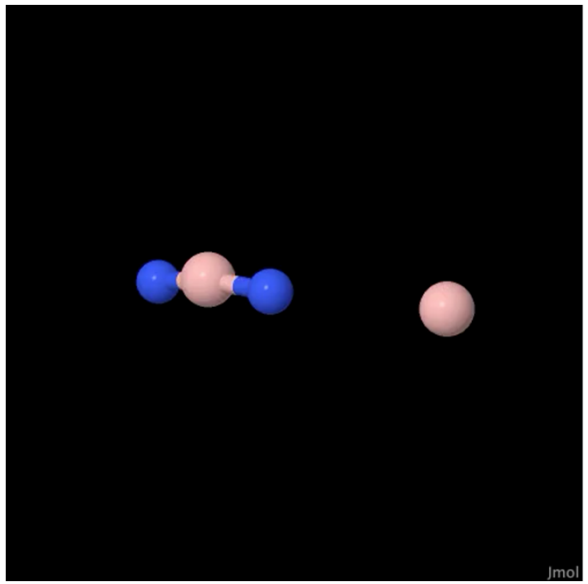

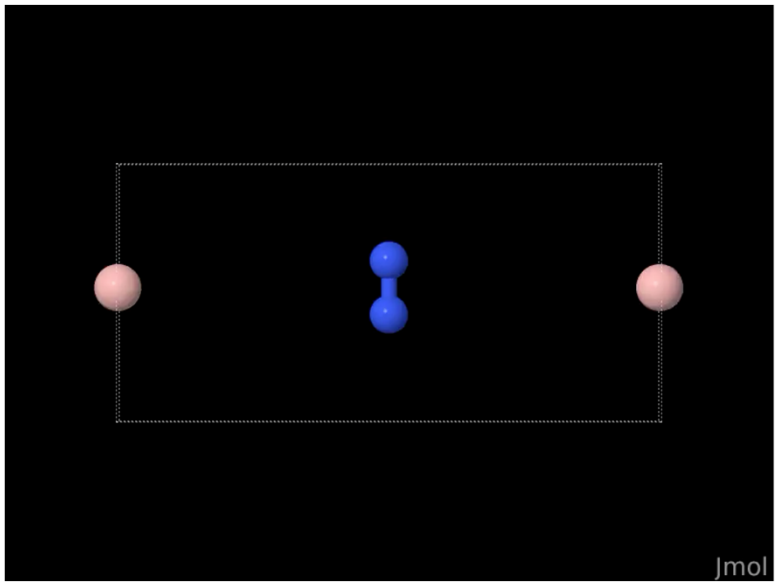

BNBN form more complex molecules

Movies: Reaction of two B_3N_3 rings to form B_6N_6 ring. and Reaction of four rings to form $B_{12}N_{12}$ ring at 2500K; O. Dwivedi, S. Jubin, S. Ethier, et *al.* (2019)

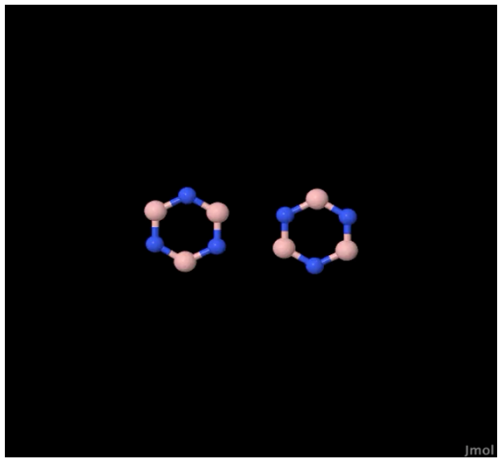

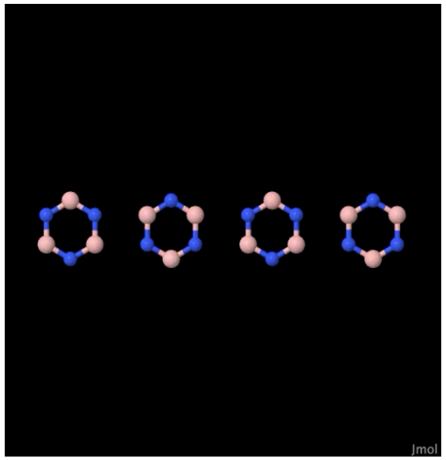

Four rings react to form $B_{12}N_{12}$ nanocage.

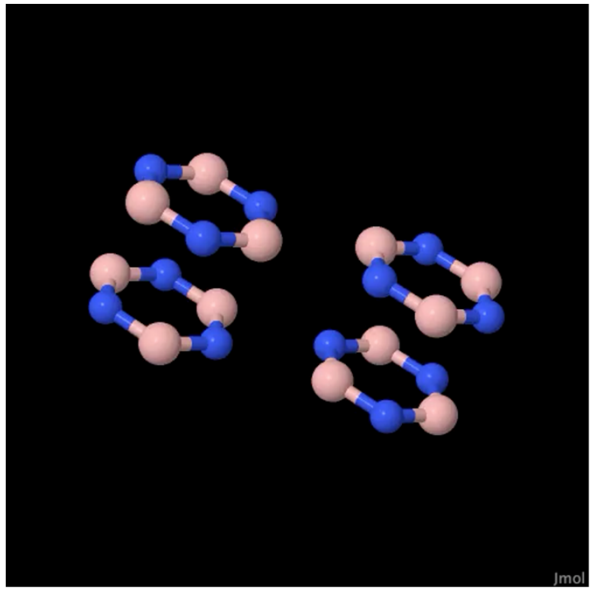

BN clusters bond energies

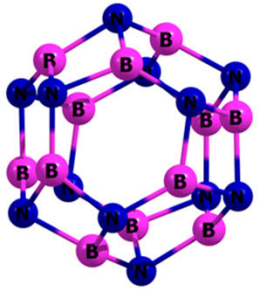

$(BN)_{12}$ Fullborene

$(BN)_{12}$ cycle chain

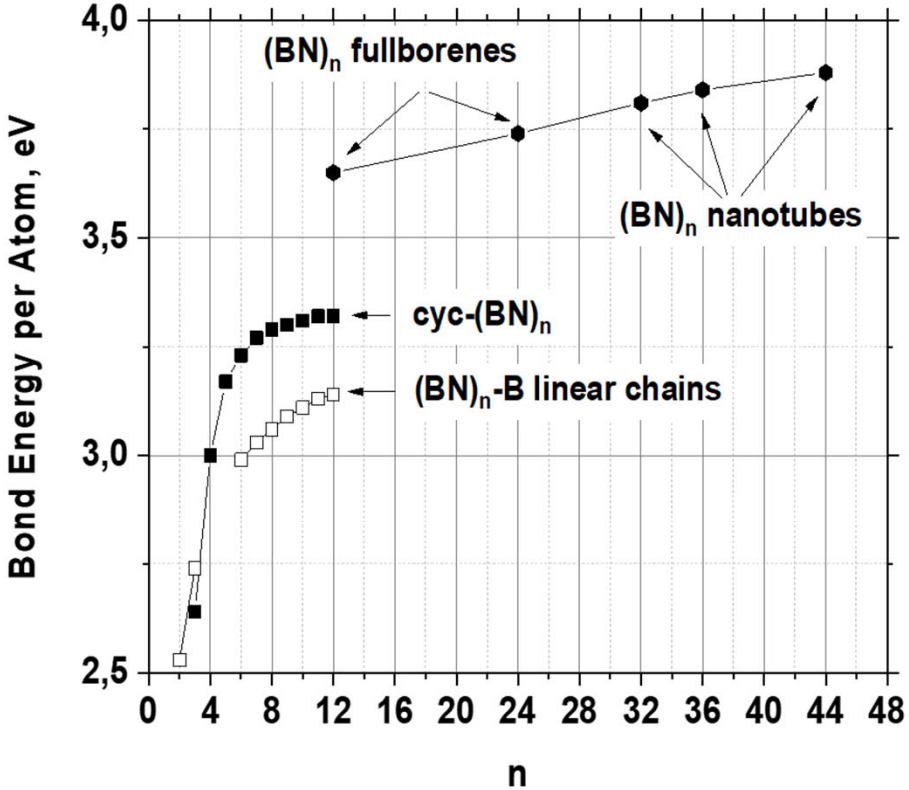

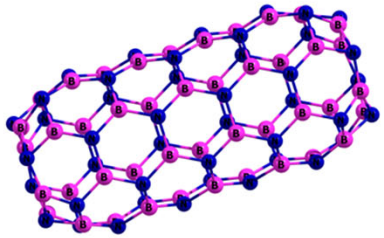

$(BN)_{44}$ nanotube

$(BN)_{12}$-B linear chain

Y. Barsukov, et *al.* (2020)

New hypothesis of BNNT synthesis

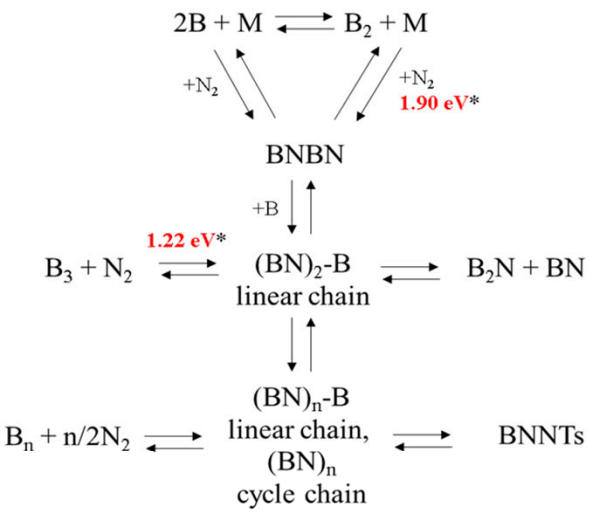

Production of B-N compounds can proceed thorough BNBN molecule formation.

Y. Barsukov, *et al.* (2020)

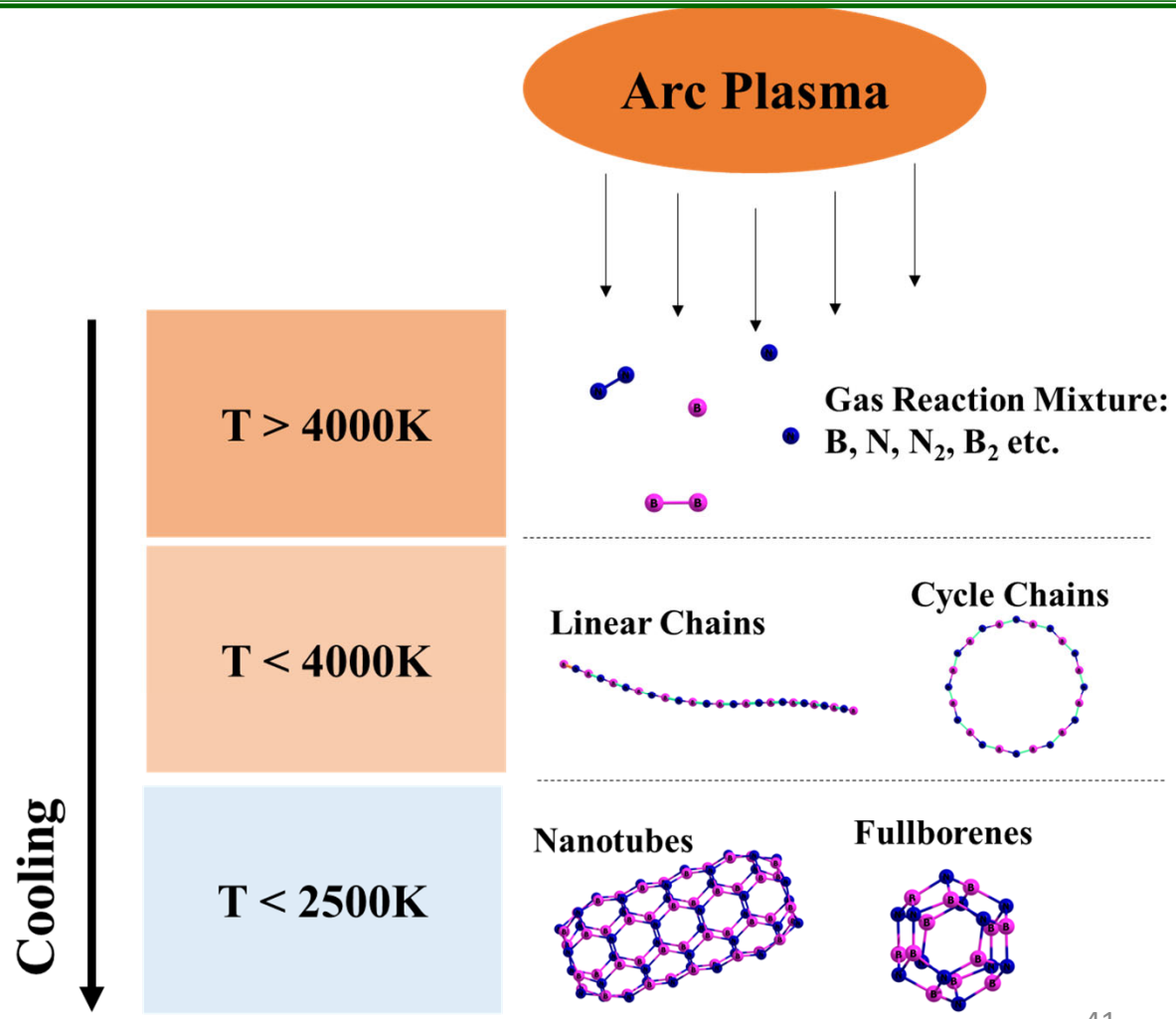

Summary: Carbon Arc

- **Developed self-consistent model of carbon arc including effects of ablation, electron emission, radiation, sheath.**
- **Model was benchmarked and validated with PPPL experimental data.**
- **Developed an analytical model which explained transition from low to high ablation regimes.**
- **Numerical simulations and analytical theory explained anodic spot formation.**
- **Showed that charging of nanotube surface affects adatom desorption and surface diffusion.**
- **DFTB modeling revealed how condensing carbon vapor forms linear chains and fullerenes during cooling implying root growth mechanism and need for metal catalyst to dissolve carbon to form carbon nanotubes.**

Summary: Boron Nitride Nanotubes

- **Formation of boron nanotube on the boron droplet has two obstacles: large energy barrier for BN cap to lift and low probability of molecular nitrogen to dissolve in boron.**
- **Fixation of N_2 molecule can proceeds through BNBN molecule formation in the B_2 + N_2 → BNBN reaction. The highest barrier of the reaction towards BNBN formation is 1.9 eV (significantly less than N_2 bond energy, 9.7 eV).**
- **The formation of BNBN molecule is energetically favourable process, because from one N_2 molecule three B-N bonds are formed in BNBN molecule. It is expected that BNBN molecule is only intermediate and complex $(BN)_n$ molecules followed by rings and then fullborenes and nanotubes will be preferably accumulated in the gas phase in equilibrium conditions as plasma cools.**
- **This gives a stronger argument that BNNTs growth can be achieved directly through BNBN molecule formation without boron droplets formation as it is accepted in the "root growth" mechanisms.**
- **Developed analytical theory for nucleation burst droplet formation.**

Acknowledgment

- **This research was supported by the U.S. Department of Energy, Office of Science, Office of Fusion Energy Sciences under contract number DE-AC02-09CH11466.**
- **The simulations have been performed using Eddy cluster of PPPL and Princeton University.**
- **Experimental colleagues: Yevgeny Raitses, Shurik Yatom, Vladislav Vekselman, Brent Stratton, Tianyuan Huang**

For those interested to use PPPL and PU diagnostics, numerical tools and facilities, please attend talk at 1pm. The upcoming solicitation for Princeton Collaborative Research Facility (PCRF) will be announced.

73rd Annual Gaseous Electronics Virtual Conference

Monday–Friday, October 5–9, 2020; Time Zone: Central Daylight Time, USA.

Session YF1: Federal Agency Perspectives in Plasma Research
1:00 PM–3:15 PM, Friday, October 9, 2020

Chair: Scott Walton, Naval Research Laboratory

Abstract: YF1.00004 : Princeton Collaborative Low Temperature Plasma Research Facility
2:15 PM–2:30 PM Live

Preview Abstract

Author:
Yevgeny Raitses
(Princeton Plasma Physics Laboratory)

Observed two ablation modes affecting synthesis of carbon nanotubes

Low ablation

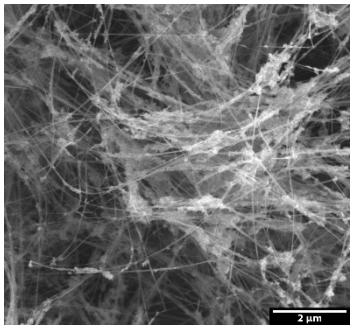

MWCNTs on the deposit

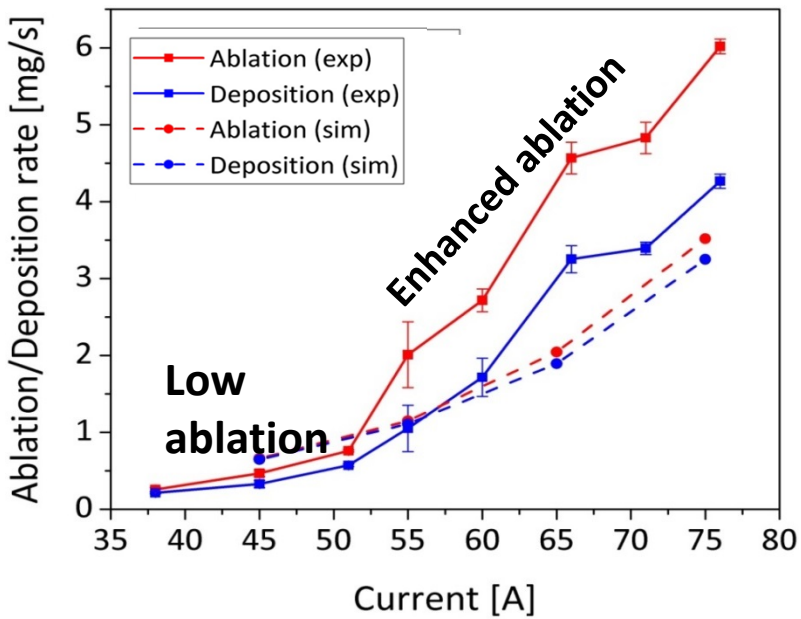

Enhanced ablation

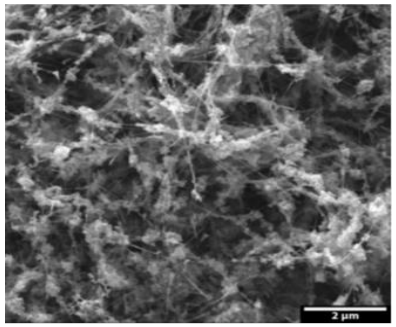

MWCNTs on the deposit

- **Correlation between synthesis selectivity, yield, and arc current:**
  - **Enhanced ablation → Higher C_2 density → Deposition with higher yield**
  - **Smaller ablation → Reduced carbon flux → Deposition with better selectivity**

Outline

37 Publications, 14 presentations are available at nano.pppl.gov

- **Nonstationary processes in arcs**

Arc oscillations affect synthesis of nanotubes

- **Synthesis of SWCNT by carbon arc with metal catalysts**
- **Metal – Carbon mixed powder filled in the hollow graphite anode rod**
- **Multi-mode oscillations: LF (10^2 Hz) and HF (10^3 Hz) modes, inside and outside the hollow anode**
- **Oscillations cause of low purity and poor selectivity of the arc synthesis**

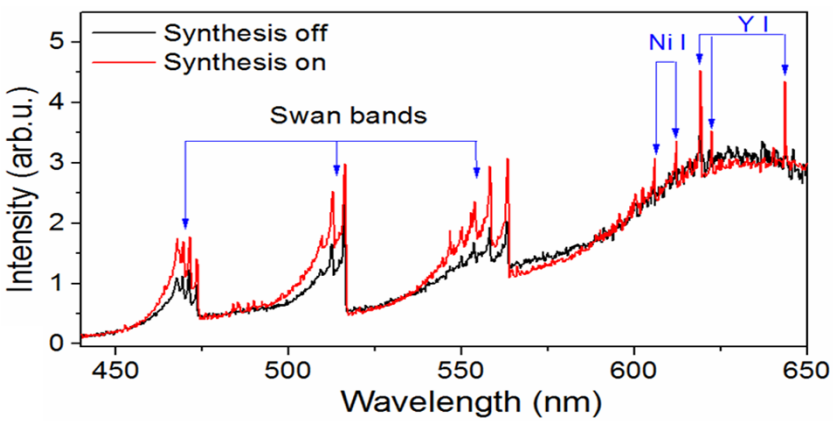

- **C_2 Filtered Fast Imaging, 10,000 fps**

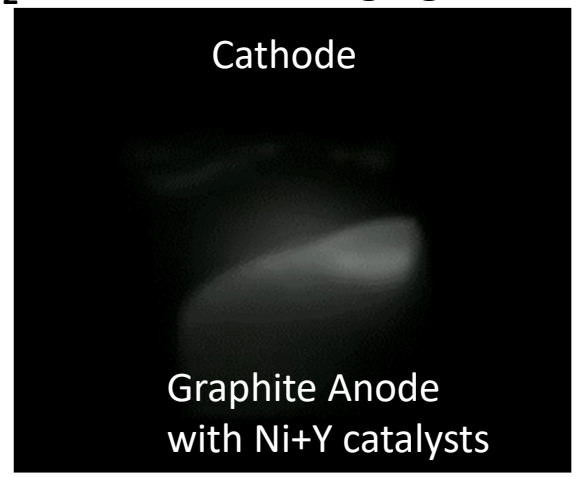

SWCNT Synthesis OFF

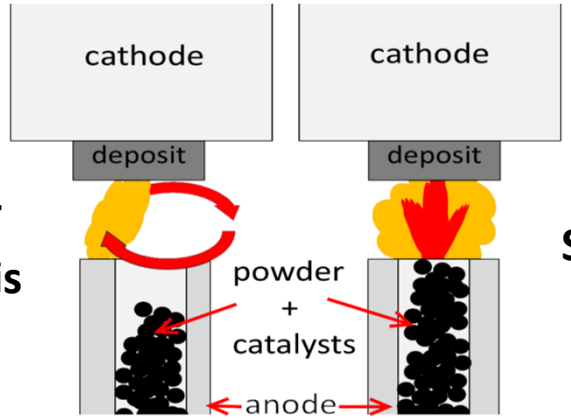

SWCNT Synthesis ON

~ 5% of time